

UNIVERSITY OF CALIFORNIA

Los Angeles

Frequency Upshifting of Electromagnetic Radiation via  
an Underdense Relativistic Ionization Front

A dissertation submitted in partial satisfaction of the  
requirements for the degree

Doctor of Philosophy in Electrical Engineering


by

Richard Lenox Savage, Jr.

1992

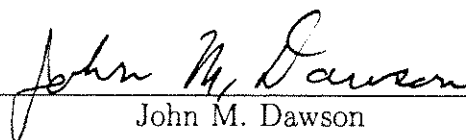
---

The dissertation of Richard Lenox Savage, Jr. is approved.



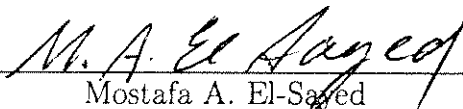
---

Francis F. Chen



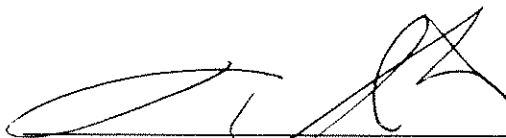
---

John M. Dawson



---

Mostafa A. El-Sayed



---

Tatsuo Itoh



---

Chandrashekar J. Joshi, Committee Chair

University of California, Los Angeles

1992

## DEDICATION

To my parents, Margaret and Richard Savage.

For Kiyomi and our son, Nathan.

# Contents

DEDICATION	iii
List of Figures	vi
ACKNOWLEDGMENTS	ix
VITA	x
ABSTRACT	xiv
1 Introduction	1
2 Theory	6
2.1 Introduction . . . . .	6
2.2 Derivation of Upshifted Frequencies in Waveguide . . . . .	7
2.2.1 Front's Frame Derivation . . . . .	7
2.2.2 Laboratory Frame Derivation . . . . .	10
2.3 Maximum Possible Upshift . . . . .	14
2.4 Derivation of Reflection and Transmission Coefficients in Waveguide	19
2.5 Derivation of upshifted Pulselengths in Waveguide . . . . .	24
2.6 "Reflection" of the <i>Backward Wave</i> . . . . .	28

<b>3</b>	<b>Experiment</b>	<b>33</b>
3.1	Resonant Microwave Cavity Set-up . . . . .	34
3.1.1	Frequency Measurements . . . . .	36
3.1.2	Interferometry Density Measurement . . . . .	39
3.1.3	Data Fit with Theory . . . . .	41
3.1.4	Detection of the <i>Backward Wave</i> . . . . .	43
3.1.5	Efficiency . . . . .	48
3.2	Unidirectional Microwave Cavity Set-up . . . . .	51
3.2.1	Grating Measurements . . . . .	53
3.2.2	Pulsewidth Measurement . . . . .	56
<b>4</b>	<b>Conclusions</b>	<b>66</b>

## List of Figures

1.1	<i>Forward wave/Backward wave convention.</i>	4
2.1	Space-time diagram for an ionization front passing through a resonant microwave cavity.	10
2.2	Detail of space time plot along the front's space-time line.	11
2.3	Front's frame view of a wave impinging upon a front of finite spatial extent.	15
2.4	High density frequency upshift vs. plasma frequency.	18
2.5	Group velocity of upshifted radiation vs. front density.	25
2.6	Expected upshifted pulse lengths vs. density.	27
2.7	Space-time diagram for a front density of $1 \times 10^{13} \text{ cm}^{-3}$ .	30
2.8	Space-time diagram for a front density of $4 \times 10^{13} \text{ cm}^{-3}$ .	31
3.1	Resonant cavity experimental setup.	34
3.2	Temporal evolution of a typical upshifted signal.	37
3.3	40 GHz, 59 GHz, 91 GHz, and 116 GHz upshifted signals vs. azulene pressure.	38
3.4	Typical interferometer signal.	40
3.5	Measured plasma density vs. azulene pressure.	41
3.6	Comparison of measured upshifted signals with theoretical predictions.	42

3.7	Forward upshifted signal at 16 mT. . . . .	44
3.8	Backward upshifted signal at 16 mT. . . . .	45
3.9	Forward upshifted signal at 71 mT. . . . .	46
3.10	Backward upshifted signal at 71 mT. . . . .	47
3.11	Antenna pattern of 40 GHz upshifted radiation. . . . .	49
3.12	Antenna pattern of 91 GHz upshifted radiation. . . . .	50
3.13	Experimental set-up with unidirectional cavity. . . . .	52
3.14	Diffraction grating frequency measurement set-up. . . . .	53
3.15	Upshifted spectra vs. azulene pressure. . . . .	54
3.16	Optimized upshifted spectrum at 46 GHz. . . . .	55
3.17	Measured density vs. azulene pressure in unidirectional waveguide. . . . .	57
3.18	Comparison of measured upshifted spectra with theoretical predic- tions. . . . .	58
3.19	Backward upshifted pulse at 4 mT azulene pressure. . . . .	59
3.20	Forward upshifted pulse at 49 mT azulene pressure. . . . .	60
3.21	Measured upshifted pulsewidths vs. density. . . . .	61
3.22	Partially eroded upshifted pulse at 10 mT azulene pressure. . . . .	62
3.23	Decayed upshifted pulse at 16 mT azulene pressure. . . . .	63
3.24	Detail of forward wave pulsewidths vs. density. . . . .	65

## ACKNOWLEDGEMENTS

There are many people to whom I am truly indebted for their inspiration, assistance, and encouragement during this research.

To Kiyomi Savage, who has been my constant companion and untiring supporter throughout these six years of graduate school. We established and achieved this goal together, and she deserves as much credit as I.

To my parents and my sister, Susan Miller, my lifeline and greatest supporters. To Chan Joshi, my thesis advisor, for his professional and personal support throughout every phase of this project, and for giving me the opportunity to be a part of such an outstanding research group.

To Warren Mori, who first recognized that underdense fronts could yield significant upshifts, for his assistance with the theory and his physical intuition in interpreting experimental results that sometimes seemed too good to be true.

To Prof. H. J. Orchard for believing in me enough to help me fight Murphy Hall and to Janice Holstein for her help waging the battle.

To Don Hopkins for his help with the early stages of the experiments and for teaching me everything I know about microwaves.

To Rob Brogle, who I hope will continue this work, for his help with the unidirectional cavity experiments, and for many long and enlightening discussions.



To Andy Sessler for his insightful and generous collaboration on this project.

To Jonathan Deeds for his help constructing the experiment (and the laboratory).

To Tudor Johnston for developing the space-time picture of the upshifting process and his assistance with the laboratory frame analysis.

To Gennady Shvets for his assistance with the derivation of the reflection and transmission coefficients in waveguide and for many helpful discussions.

To Ken Marsh, who first told me that a professor named Joshi was interested in building a femtosecond laser laboratory, for his sound advice and assistance including late nights giving practice plasma physics oral exams.

To Chris Clayton for his example of an experimental scientist and his many helpful suggestions.

To Frank Chen, who gave me my first job in a research laboratory, for his friendship and support over all these years and for his concern for all of the details.

To Tom Katsouleas, Scott Wilks, and John Dawson for their constant enthusiasm toward and support of these experiments.

To Don Prosnitz of LLNL for the loan of microwave equipment.

To Harold Fetterman, who encouraged me to return to graduate school six years ago, and has shared both the good and bad parts of the journey.

And finally to Gabriel Rebeiz, Jeff Corbett, Dan Goebel, Brian Perrochet, John Howard, Marc Day, Zak Sandler, Rob van den Berg, Tatsuo Shoji, Robert Shih, Lee Cardenas, Xuan Nguyen, Scott Burns, Dorothy Tarkington, Tony Peebles, Wim Leemans, Maria Guerrero, Pepe Davis, Garnick Hairapetian, Chris Decker, Amit Lal, Matt Everett, Youichi Sakawa, and Mei-Tai Shu, for the friendships that made this trek possible and worthwhile.

## VITA

- July 7, 1954      Born, Enid, Oklahoma
- 1978              B.S., Physics, University of California, Los Angeles.
- 1978 - 1986      Development Engineer, Electrical Engineering Department, University of California, Los Angeles.
- 1988              M.S., Electrical Engineering, University of California, Los Angeles.
- 1989              Teaching Assistant, Electrical Engineering Department, University of California, Los Angeles
- 1992              IEEE Nuclear and Plasma Sciences Society, 1991 Graduate Scholarship Award
- 1986 - 1992      Graduate Research Engineer, Electrical Engineering Department, University of California, Los Angeles.

## PUBLICATIONS AND PRESENTATIONS

- C. Joshi, C. E. Clayton, K. Marsh, Y. Sakawa, and R. L. Savage Jr.  
"Evidence for periodic breakup of a radially modulated  $0.35\mu\text{m}$  laser beam due to thermal self-focusing in a plasma," *Opt. Commun.*, vol. 70, pp. 44-49, 1989.
- Y. Kitagawa, R. L. Savage Jr. and C. Joshi  
"Demonstration of collisionally enhanced degenerate four-wave mixing in a plasma," *Phys. Rev. Lett.*, vol. 62, pp. 151-154, 1989.

- R. L. Savage Jr. Y. Kitagawa, and C. Joshi,  
"Collisionally enhanced degenerate four-wave mixing in a plasma." Paper presented at the Conference on Lasers and Electro-Optics, Baltimore, MD, April 24-28, 1989.
- R. L. Savage Jr. C. Joshi, and W. B. Mori  
"Demonstration of frequency upshifting of electromagnetic radiation by a relativistic ionization front." Paper presented at the Twentieth Annual Anomalous Absorption Conference, Traverse City, MI, July 9-13, 1990.
- R. L. Savage Jr. C. Joshi, and W. B. Mori  
"Frequency upconversion of electromagnetic radiation via interaction with a laser-produced ionization front." Paper presented at the American Physical Society Sixth Interdisciplinary Laser Science Conference, Minneapolis, MN, September 16-19, 1990.
- R. L. Savage Jr. C. Joshi, and W. B. Mori  
"Experimental observation of large frequency upshifts from underdense ionization fronts." Paper presented at the Thirty-Second Annual Meeting of the American Physical Society Division of Plasma Physics, Cincinnati, OH, November 12-16, 1990.
- R. L. Savage Jr. W. B. Mori, C. Joshi, T. W. Johnston, and G. Shvets  
"Tunable radiation generation using underdense ionization fronts." Invited paper presented at the International Conference on Research Trends in Coherent Radiation Generation and Particle Accelerators, La Jolla, CA, February 11-13, 1991. To be published in *Research Trends in Physics*.
- R. L. Savage Jr. C. Joshi, and W. B. Mori  
"Recent results from the relativistic ionization front experiment." Paper presented at the Twenty-First Annual Anomalous Absorption Conference, Banff, Alberta, Canada, April 14-19, 1991.

- R. L. Savage Jr. C. Joshi, and W. B. Mori  
"Generation of highly tunable microwave radiation via a relativistic ionization front," in *Proc. IEEE MTT-S Int. Microwave Symp.*, Boston, MA, 1991.
- R. L. Savage Jr. C. Joshi, and W. B. Mori  
"Tunable high frequency radiation source utilizing a relativistically propagating ionization front." Invited paper presented at the 1991 LEOS Summer Topical Meeting on Optical Millimeter-Wave Interactions: Measurements, Generation, Transmission and Control, Newport Beach, CA, July 24-26, 1991
- R. L. Savage Jr. C. Joshi, and W. B. Mori  
"Tunable high frequency radiation source utilizing a relativistically propagating ionization front," in *Proc. Int. Symp. Space Terahertz Tech.*, Pasadena, CA, 1991.
- R. L. Savage Jr. T. W. Johnston, W. B. Mori, C. Joshi  
"Generation of short pulses of tunable millimeter-wave radiation by a laser produced ionization front." Paper presented at the Thirty-Third Annual Meeting of the American Physical Society Division of Plasma Physics, Tampa, FL, November 4-8, 1991.
- R. L. Savage Jr. C. Joshi, and W. B. Mori  
"Frequency upconversion of electromagnetic radiation upon transmission into an ionization front," *Phys. Rev. Lett.*, vol. 68, pp. 946-949, 1992.
- R. L. Savage Jr. R. P. Brogle, W. B. Mori, and C. Joshi  
"Photon acceleration via laser-produced ionization fronts." Paper presented at the Eighth International Conference on Ultrafast Phenomena, Antibes-Juan les Pins, France, June 8-12, 1992.

R. L. Savage Jr. R. P. Brogle, W. B. Mori, and C. Joshi

“Frequency upshifting and pulse compression via underdense relativistic ionization fronts.” Invited paper to be published in the *IEEE Trans. Plasma Sci.* special issue on *Coherent radiation generation using plasmas*, February, 1993.

ABSTRACT OF THE DISSERTATION

Frequency Upshifting of Electromagnetic Radiation via  
an Underdense Relativistic Ionization Front

by

Richard Lenox Savage, Jr.

Doctor of Philosophy in Electrical Engineering

University of California, Los Angeles, 1992

Professor Chandrashekhar J. Joshi, Chair

An underdense, relativistically propagating ionization front has been utilized to upshift the frequency of an impinging electromagnetic wave from 35 GHz to more than 173 GHz in a continuously tunable fashion. The source radiation interacted with the ionization front inside a metallic waveguide. The front, simply a moving boundary between ionized and neutral gas, was created as a short, intense pulse of ionizing laser radiation propagated through the gas-filled waveguide.

In 1991, W. B. Mori showed theoretically that large upshifts are possible using underdense ionization fronts (underdense implies that the plasma density is lower than that required to reflect the source radiation), where the source wave is transmitted through the plasma/neutral boundary. We have extrapolated Mori's analysis to interactions within a waveguide. We launched source radiation both along and opposite to the direction of propagation of the front. Because the group velocity of the source radiation inside the waveguide was only half that

of the ionization front, both the counter- and co-propagating source radiation were overtaken and transmitted into the front. In agreement with the theoretical predictions, the co-propagating wave was upshifted to a higher frequency than the counter-propagating wave for a given plasma density, and both upshifts were proportional to the front's density.

The theory also predicts temporal compression of the co-propagating wave as its group velocity increases with frequency. Conversely, the group velocity of the counter-propagating wave is expected to decrease to zero, then increase in the same direction as the front for higher densities, also being significantly compressed for large upshifts. We have experimentally observed the compression of the co-propagating wave to less than 500 psec duration, in good agreement with theory. The duration of the upshifted counter-propagating wave initially increased with plasma density to more than 7 nsec and was less than 2 nsec at higher densities. However, the "reflection" of the counter-propagating wave was not conclusively resolved.

This is a new technique for generating high-power, short-pulse, tunable radiation, and has potential applications in areas such as time-resolved microwave spectroscopy, plasma diagnostics, and remote sensing.

# Chapter 1

## Introduction

When a pulse of electromagnetic radiation reflects from a moving mirror, both its frequency and its duration are altered by the relativistic Doppler effect [1] which depends strongly on the velocity of the mirror. It has been predicted that similar changes would occur if the radiation were to reflect from a moving plasma/neutral gas boundary, an ionization front [2, 3]. An ionization front is created, for instance, when an ionizing laser pulse passes through a region of neutral gas. The Doppler shift is the same in both cases, but unlike the mirror, the ionization front has no kinetic energy. Therefore, in contrast to the moving mirror, the number of photons is not conserved upon reflection from the front, and the energy in the reflected pulse may be much less than the incident pulse energy. In order to reflect the impinging radiation, the front must be overdense; that is, the density of the plasma in the front must be above the critical density for electromagnetic radiation *when viewed from the rest frame of the front*. The critical density is defined as that density for which the characteristic plasma frequency,  $\omega_p$ , equals the radiation frequency. The plasma frequency is defined



by

$$\omega_p = \left[ \frac{4\pi n_0 e^2}{m} \right]^{1/2} \quad (1.1)$$

where  $n_0$  is the plasma density,  $m$  is the electron's mass, and  $e$  is its charge. Because the frequency of the incident radiation is higher when viewed from this frame and the plasma frequency is Lorentz invariant, creation of an overdense front requires that the plasma be more dense than for a stationary boundary. Thus creation of an overdense front is often technologically impracticable. However, it has recently been predicted that large frequency upshifts and pulse compressions are possible even for *underdense* relativistic fronts, where the incident radiation is transmitted into the plasma [4]. In this case the degree of frequency upshift is proportional to the plasma density, and unlike reflection from an overdense front, is relatively insensitive to the front's velocity.

Developments in laser technology have enabled the generation of relativistically propagating ionization fronts by intense short-pulse lasers via photo-ionization. Several groups have reported that either a portion of the ionizing radiation or a separate probe pulse was blue-shifted as it co-propagated with the front [5, 6, 7]. This upshifting results from phase modulation due to the rapid formation of the plasma as the radiation propagates with the density gradient at the plasma/neutral gas boundary (see section 2.3). Novel radiation sources utilizing similar co-propagating ionization fronts or relativistic plasma waves have been proposed [8, 9, 10]. To obtain large upshifts, these schemes require that the upshifting radiation and the density gradient co-propagate over a considerable distance. Conversely, in a geometry in which radiation impinges upon the front, the radiation and the front need not propagate at the same velocity. The ultimate upshift in this case depends only on the maximum density in the front,

and is acquired in a relatively short interaction region. Furthermore, for large upshifts the incident pulse is significantly reduced in duration [4], as is the case for reflection from overdense fronts [3, 11].

Using a fixed-frequency source for the incident radiation and an ionizing laser with a fixed output, one can create a tunable source of upshifted radiation by simply varying the neutral gas density in the interaction region. The frequency of the upshifted radiation can be continuously tuned to many times the source frequency. Furthermore, because the upshifted pulse is generated only during the transit time of the laser pulse through the interaction region (and may be compressed to much less than the transit time), the upshifted pulse can be very short in duration even if the source gives much longer output pulses or even continuous output. Tunable, short-pulse radiation sources derived from this technique have potential applications in many areas, including plasma diagnostics, spectroscopy, and remote sensing.

The goal of this work was to test the predictions of the underdense ionization front theory, and in doing so to create a new type of tunable radiation source. Our experiments utilize a fixed-frequency source of microwave radiation operating at approximately 35 GHz. The front is created by a 50-psec-long ionizing laser pulse. The interaction occurs inside a metallic waveguide where the group velocity of the source radiation is about half of the free space value,  $c$ . The metallic waveguide is used to reduce the transverse spatial extent of the source wave. Reducing the volume of the interaction region allows one to achieve a higher front density for a fixed ionizing laser energy. Operating close to the cutoff frequency of the waveguide such that the group velocity of the source radiation is only  $.5c$  allows additional opportunities to test the theory. In free space with the source and

ionizing radiation propagating collinearly, they will only interact with each other when they are counter-propagating. This is because the front will propagate at approximately the group velocity of the ionizing laser radiation in the plasma it has created, which must be less than  $c$ . However, when the group velocity of the source radiation is less than  $c$ , it can interact with the front even when they co-propagate (the source radiation will be overtaken by the front). Theory predicts that for a given plasma density the degree of upshift in the co-propagating geometry will be greater than in the counter-propagating case. In both cases the degree of upshift will be proportional to the plasma density in the front.

We refer to radiation which is initially propagating in the same direction as the front, and is thus overtaken, as a *forward* wave. Radiation which is initially counter-propagating with respect to the laser pulse is referred to as a *backward* wave (see Fig. 1.1). Theory predicts that the group velocity of a forward wave will

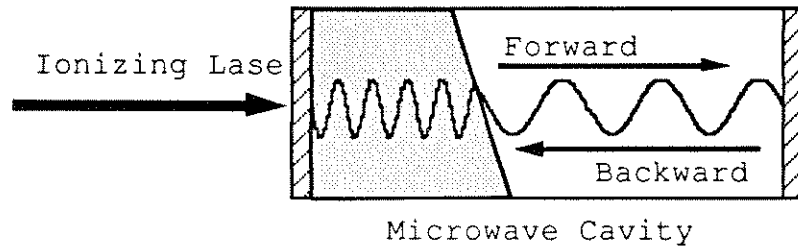


Figure 1.1: *Forward wave/Backward wave convention.*

always increase as it is upshifted by its interaction with the ionization front. Thus for large upshifts, the upshifted wave will follow along closely behind the front, leading to significant compression of the duration of the upshifted radiation. On the other hand, in the counter-propagating case the group velocity of the backward wave initially decreases as it is upshifted. This leads to an increase in its duration. Stated another way, the increase in the frequency of the forward

wave is always greater than the increase in the cutoff frequency of the waveguide as it is filled with plasma. Thus the upshifted forward radiation is always farther from cutoff than the source radiation, and its group velocity is closer to  $c$ . Initially, it is just the opposite for the backward wave. In fact, as the plasma density in the front increases the group velocity of the backward wave approaches zero. Theory predicts that as the density of the front increases further, the backward wave begins to propagate in the same direction as the front. The group velocity of this turned-around backward wave increases with plasma density, and the wave is also significantly compressed in duration for large upshifts.

In our experiments we have upshifted the 35 GHz source radiation to more than 173 GHz. Using microwave interferometry to measure the spatially-averaged plasma density in the interaction region, we have confirmed that the upshift is proportional to front density, as predicted. We have measured the duration of the upshifted pulses with better than 1 nsec resolution. The measured pulse lengths are in reasonable agreement with the theoretical predictions for both the forward and backward waves. We have observed the duration of the backward wave increasing with increasing plasma density, but have been unable to access the density regime where the backward wave should turn around and have a high group velocity in the forward direction. The observation of this “reflected” backward wave remains a critical test of the theory of underdense ionization fronts.

## Chapter 2

### Theory

#### 2.1 Introduction

The early theoretical work in this area concentrated on reflection from overdense ionization fronts [2, 3]. More recently, frequency upshifting by co-propagating ionization fronts has been studied as well [8, 9]. In 1991 W. B. Mori showed theoretically that underdense ionization fronts can significantly increase the frequency and compress the duration of impinging electromagnetic radiation [4]. We extend his theoretical analysis to the case where the front and the source radiation interact inside a metallic waveguide. We derive the expected upshifted frequencies for the forward and backward waves in both the rest frame of the ionization front (as Mori did) and in the laboratory frame using a space-time analysis of the upshifting process. We also derive the reflection and transmission coefficients for the waveguide case, including the coefficient for the static, spatially-periodic magnetic field that is left behind in the plasma (the free streaming mode in the front's frame). Finally, we pay special attention to the proposed laboratory frame "reflection" of the transmitted backward wave into the direction of propagation of the front.

## 2.2 Derivation of Upshifted Frequencies in Waveguide

The derivation of the upshifted frequencies can be carried out either in the laboratory frame or in the rest frame of the ionization front. By making a Lorentz transformation to the front's rest frame, the derivation is simplified to that of a stationary boundary with neutral gas and a higher frequency electromagnetic wave impinging upon it from one side and plasma and the upshifted radiation streaming away on the other. However, in certain geometries the front may propagate faster than the speed of light, in which case Lorentz transformations to the front's frame are impossible. This does not contradict any physical principles; the front is simply the boundary at which the ionization takes place, and therefore carries no information or energy. Because one cannot Lorentz-transform to a frame moving faster than  $c$ , the analysis for super-luminous fronts is simplest in the laboratory frame [3]. We use space-time plots for our laboratory frame analysis because they help one to visualize the upshifting and pulse compression over the full range of front velocities, from stationary to infinitely fast ("flash ionization" [13, 14, 15]).

### 2.2.1 Front's Frame Derivation

Consider a long microwave cavity of unspecified cross section containing counter-propagating microwave radiation (a standing wave, for example), a forward and a backward wave. An ionizing laser pulse passes along the axis of the cavity creating an underdense, relativistically-propagating ionization front. Before the arrival of the laser pulse, the forward and backward radiation have the same

frequency,  $\omega_f = \omega_b = \omega$ . The magnitude of their oppositely directed wave vectors is determined by the dispersion relation for electromagnetic radiation in the uniform waveguide,  $\omega^2 = \omega_c^2 + c^2 k_{f,b}^2$ , where  $\omega_c$  (Lorentz invariant along the waveguide axis) is the cutoff frequency for the particular operating mode. They both propagate at the group velocity,  $v_g = c(1 - \omega_c^2/\omega^2)^{1/2}$ , which can be significantly less than  $c$  for  $\omega$  close to  $\omega_c$ . If we neglect depletion of the ionizing laser pulse, and assume that its frequency,  $\omega_l$ , is much higher than the cutoff frequencies of the waveguide modes ( $\omega_l \gg \omega_c$ ), then the front propagates at approximately the velocity of the ionizing laser pulse in the plasma. This velocity, given by

$$v_{front} \simeq c \left\{ 1 - (\omega_c^2 + \omega_p^2)/\omega_l^2 \right\}^{1/2}, \quad (2.1)$$

can be very close to  $c$ . Here we assume that the laser is primarily in the same mode as the microwave radiation. In reality, the laser radiation is probably not guided and  $\omega_c$  can be omitted from Eq. 2.1.

The front's frame derivation proceeds by first making a Lorentz transformation to the rest frame of the ionization front. As mentioned earlier, in this frame the front is a stationary boundary with neutral gas streaming toward it on one side and plasma streaming away from it at  $v_{front}$  on the other. When  $v_g < v_{front}$  both the forward and the backward waves propagate toward the front with frequencies in this frame given by  $\omega'_f = \omega\gamma(1 \mp \beta v_g/c)$ . Here  $\gamma \equiv (1 - \beta^2)^{-1/2}$  is the relativistic Lorentz factor for the front, and  $\beta \equiv v_{front}/c$ . If  $(\omega_p^2 + \omega_c^2)^{1/2} < \omega'_{f,b}$ , then the front is underdense and the radiation is transmitted into it. As with any stationary boundary, the transmitted radiation has the same frequency as the incident radiation, but its wave number adjusts to obey the dispersion relation for electromagnetic radiation in the streaming plasma, namely  $\omega_{plasma,f,b}^2 =$

$\omega_c^2 + \omega_p^2 + c^2 k_{plasma_{f,b}}'^2$ . Thus, inside the plasma in the front's frame we have  $\omega'_{plasma_{f,b}} = \omega'_{f,b}$  and  $k'_{plasma_{f,b}} = (1/c)(\omega_{f,b}'^2 - \omega_c^2 - \omega_p^2)^{1/2}$ . To evaluate the frequencies of the upshifted radiation in the plasma in the laboratory frame, we now Lorentz transform back and obtain

$$\omega_{plasma_{f,b}} = \omega'_{plasma_{f,b}} \gamma \left\{ 1 - \beta \left( 1 - \frac{\omega_c^2 + \omega_p^2}{\omega_{plasma_{f,b}}'^2} \right)^{1/2} \right\}. \quad (2.2)$$

Because all of the cavity and plasma boundaries are stationary in the laboratory frame, the frequency of the radiation will not change as it leaves the cavity (see Section 2.6). For underdense fronts ( $(\omega_p^2 + \omega_c^2)^{1/2} \ll \omega'_b$ ), Eq. 2.2 can be expanded to give

$$\omega_{plasma_f} \approx \frac{\omega}{2} (1 \mp \beta v_g/c) \left\{ 1 + \frac{\omega_c^2 + \omega_p^2}{\omega^2 (1 \mp \beta v_g/c)^2} \right\}. \quad (2.3)$$

Similarly, the upshifted wave numbers in the laboratory frame are

$$k_{plasma_f} \approx \frac{\omega}{2c} (1 \mp \beta v_g/c) \left\{ 1 - \frac{\omega_c^2 + \omega_p^2}{\omega^2 (1 \mp \beta v_g/c)^2} \right\}. \quad (2.4)$$

It follows from Eq. 2.3 that the upshifted frequencies increase linearly with plasma density and that  $\omega_{plasma_f}$  is always greater than  $\omega_{plasma_b}$ . For highly relativistic fronts,  $\beta \approx 1$ , and the degree of upshift is independent of  $v_{front}$ , depending only on the plasma density. The forward wave always propagates in the forward direction;  $k_{plasma_f}$  is always negative. On the other hand,  $k_{plasma_b}$  changes sign when the term in brackets in Eq. 2.4 changes sign. Therefore, as the front's density increases, the backward wave's group velocity decreases to zero then increases in the forward direction. This occurs when the group velocity of the backward wave in the front's frame is less than  $v_{front}$  [4]. This type of "reflection" from an underdense front can give rise to large frequency upshifts and temporal compressions that are much different than those predicted by the usual Doppler effect. This topic will be discussed further in Section 2.6.



## 2.2.2 Laboratory Frame Derivation

We now present a laboratory frame analysis using space-time diagrams. Fig. 2.1 is a space-time plot for an ionization front interacting with radiation confined within a microwave cavity operating near cutoff. The ionizing laser pulse, which

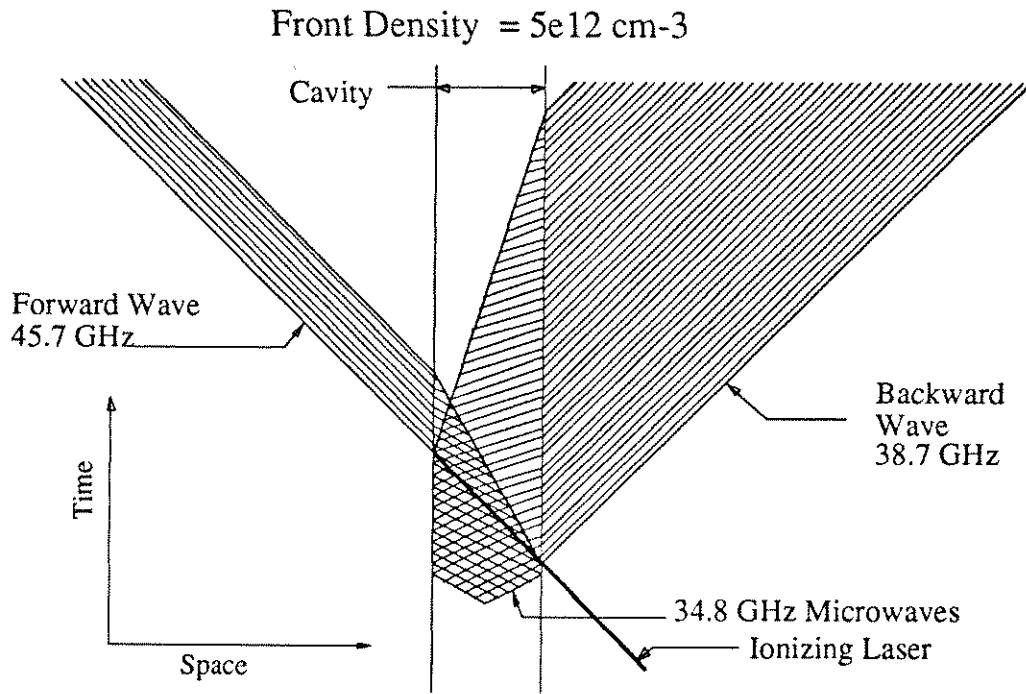


Figure 2.1: Space-time diagram for an ionization front passing through a resonant microwave cavity.

passes through the cavity from right to left, is propagating at approximately  $c$ , and is represented by the thick line at 45 degrees to the space and time axes. The parallel vertical lines in the figure represent the stationary cavity windows from which a portion of the circulating microwave radiation reflects before the arrival of the laser pulse. The group velocity of the circulating radiation inside the cavity,  $v_g$ , is  $.5c$ . The parallel sets of lines between the cavity windows and below the laser pulse's space-time line in Fig. 2.1 show the propagation along the

cavity axis of points of equal phase in the source radiation. Because the product of the group velocity and the phase velocity,  $v_p$ , is  $c^2$ , the phase velocity of the source radiation, given by the inverse of the slope of the parallel lines, is greater than  $c$ .

As the source radiation is transmitted into the underdense front, its frequency is upshifted. The degree of upshift can easily be derived by taking a close look at the interaction of the radiation with the moving boundary. Fig. 2.2 shows a

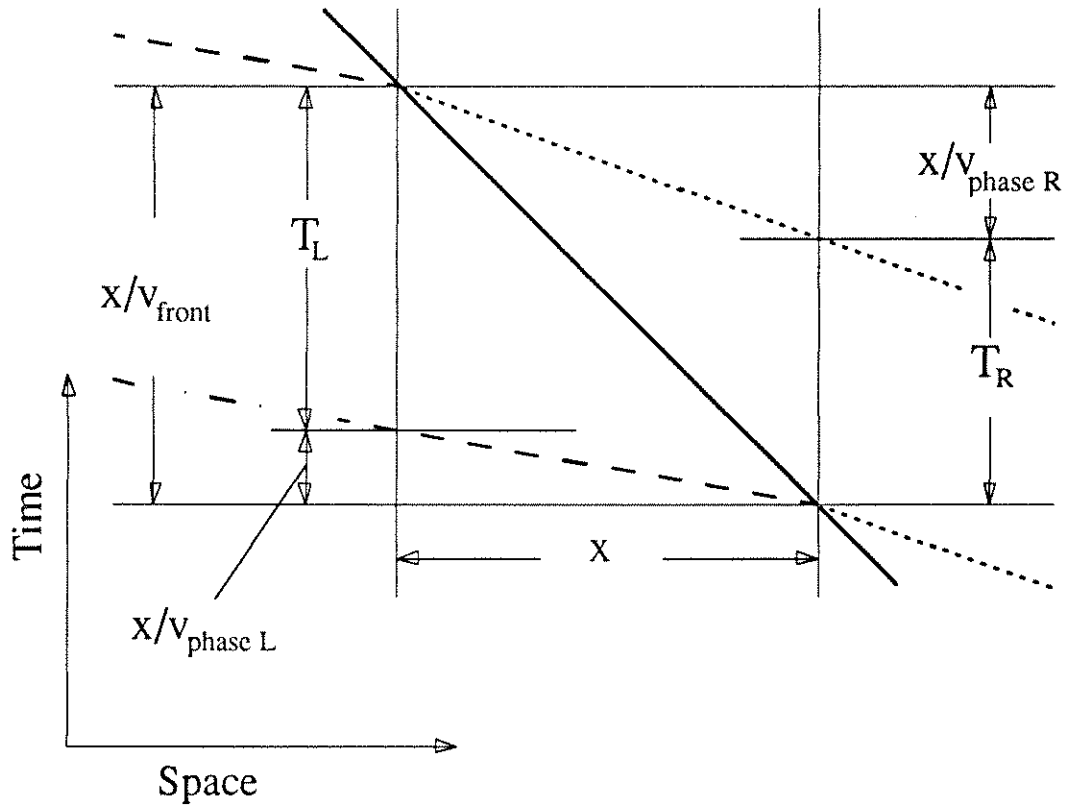


Figure 2.2: Detail of Fig. 2.1 along the ionization front's space-time line for the *forward* radiation.

magnified detail of Fig. 2.1 along the front's space-time line. The parallel dashed lines track points of constant phase for the radiation inside the cavity that is

propagating in the same direction as, and being overtaken by, the ionization front, the forward wave. The parallel dotted lines track points of constant phase for the upshifted, transmitted radiation. The derivation proceeds from three simple requirements: 1) the source radiation must obey the dispersion relation (Lorentz-invariant in our geometry) for an electromagnetic wave in a conducting waveguide,  $\omega^2 = \omega_c^2 + c^2 k^2$ , where  $\omega_c$  is the cutoff frequency for the particular operating mode in the waveguide; 2) the number of cycles of the source radiation impinging on the front must equal the number of cycles of upshifted radiation leaving the front; and 3) the upshifted radiation must obey the dispersion relation for an electromagnetic wave in a plasma filled waveguide (also Lorentz-invariant),  $\omega_{up}^2 = \omega_c^2 + \omega_p^2 + c^2 k^2$ , where  $\omega_p$  is the plasma frequency. The first and third requirements thus dictate the slope of the parallel lines between the cavity windows below and above the front's space-time line in Fig. 2.2, and the second requirement is simply that the spacing between the lines, measured along the front's space-time line, must be equal on both sides.

The full range of front velocities can be considered by simply changing the slope of the front's space-time line. The two limiting cases are a stationary boundary and one that propagates at an infinitely high velocity. For the stationary boundary, the front's space-time line is vertical and requirement 2 is simply that the frequency is fixed. As is the usual case for stationary interfaces, the wave number must adjust itself in order to obey requirement 3. For the infinitely fast front, also known as "flash ionization" [13], the boundary is horizontal in the space-time plot. Thus, the wave number is fixed by requirement 2 and the frequency adjusts in order to satisfy requirement 3.

It can easily be seen in Fig. 2.2 that the temporal periods of the radiation on

the left and right sides of the front are given by

$$T_L = \frac{2\pi}{\omega_L} = X \left( \frac{1}{v_{front}} - \frac{1}{v_{phase_L}} \right) \quad (2.5)$$

and

$$T_R = \frac{2\pi}{\omega_L} = X \left( \frac{1}{v_{front}} - \frac{1}{v_{phase_R}} \right). \quad (2.6)$$

Using these expressions, we can write the upshifted frequency as a function of the source frequency as

$$\omega_R = \omega_L \frac{(1/v_{front} - 1/v_{phase_L})}{(1/v_{front} - 1/v_{phase_R})}. \quad (2.7)$$

Viewed another way, this relationship follows from the requirement that the phase be continuous across the boundary, which is a consequence of the requirement that E and B be continuous at the front. The dispersion relations to the left of (before) and to the right of (after) the front are

$$\omega_L^2 = \omega_c^2 + c^2 k_L^2 \quad (2.8)$$

and

$$\omega_R^2 = \omega_c^2 + \omega_p^2 + c^2 k_R^2. \quad (2.9)$$

By eliminating  $k_R$  and  $k_L$  from the above expressions, we obtain a quadratic equation in  $\omega_R$  which can be solved to give

$$\omega_R = \omega_L \gamma^2 (1 - \beta v_g/c) \left\{ 1 - \beta \left[ 1 - \frac{\omega_c^2 + \omega_p^2}{\omega_L^2 \gamma^2 (1 - \beta v_g/c)^2} \right]^{\frac{1}{2}} \right\}. \quad (2.10)$$

Here  $\beta = v_{front}/c$  and  $\gamma = (1 - \beta^2)^{-1/2}$  is the relativistic Lorentz factor associated with the front.  $v_g$  is the group velocity of the source radiation in the cavity, and is related to  $v_{phase_L}$  by  $v_g v_{phase_L} = c^2$ . A similar derivation for the radiation inside the cavity which is propagating in the opposite direction to the ionization front

(left to right in Fig. 2.1), the backward wave, yields an upshifted frequency given by

$$\omega_R = \omega_L \gamma^2 (1 + \beta v_g/c) \left\{ 1 - \beta \left[ 1 - \frac{\omega_c^2 + \omega_p^2}{\omega_L^2 \gamma^2 (1 + \beta v_g/c)^2} \right]^{\frac{1}{2}} \right\}. \quad (2.11)$$

The upshifted forward wave is shown by the parallel lines above and to the left of the front's line in Fig. 2.1, and the backward wave is shown by the parallel lines above and to the right. These lines represent the propagation of points of equal phase, and are bounded by lines which represent the group velocity of the radiation. Eq. 2.10 and Eq. 2.11 both predict upshifted frequencies that are proportional to the front density, with the forward wave always upshifted to a higher frequency than that of the backward wave for a given plasma density. We note that  $\beta$  is not limited to being less than unity, in fact, we recover the flash-ionization results for  $\beta \rightarrow \infty$  [13]. Eqs. 2.10 and 2.11 give exactly the same result as Eq. 2.2, as expected.

### 2.3 Maximum Possible Upshift

To derive the maximum possible upshift for both underdense and overdense ionization fronts, consider a wave impinging upon a front of finite spatial extent. Viewed from the front's frame, it is simply a wave propagating toward a stationary density gradient. This is illustrated in Fig. 2.3 where the interaction is represented in the front's frame by a ball (wave) rolling toward a hill (ionization front). Following our previous convention, the incident wave frequency in this frame is  $\omega'_f = \omega \gamma (1 \mp \beta v_g/c)$ , as before. For an underdense front, the velocity of the wave (ball) decreases as it propagates into the front (up the hill) as shown in Fig. 2.3a. For higher density fronts, the wave will propagate into the density

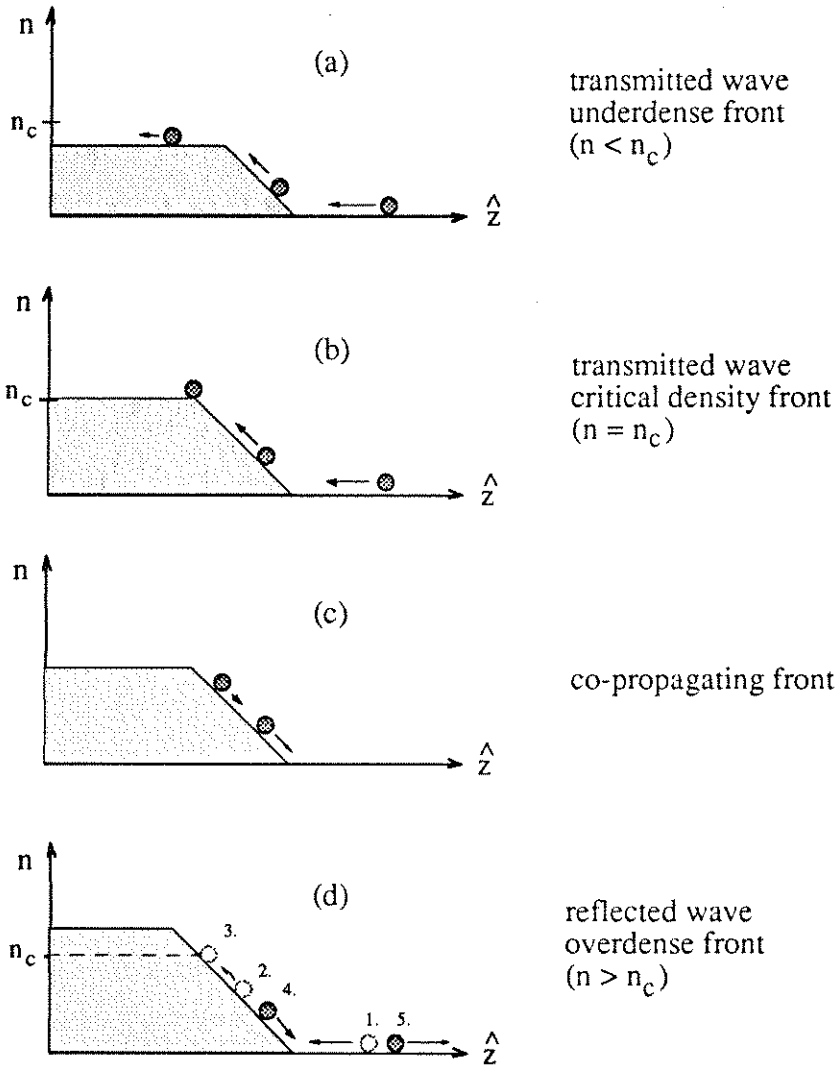


Figure 2.3: Front's frame view of a wave impinging upon a front of finite spatial extent (a stationary density gradient in this frame). a) a wave transmitted into an underdense front b) a transmitted wave propagating to a point where the group velocity is zero - a critical density front c) a reflected wave propagating back down the density gradient - a co-propagating front d) a wave reflected by an overdense front.

gradient until it reaches the point where the plasma density is equal to the critical density,  $n_c$ ; that is, when  $\omega'_b = (\omega_c^2 + \omega_p^2)^{1/2}$  (see Fig. 2.3b). This density separates the underdense and overdense regimes. At this density the group velocity of the radiation in this frame goes to zero.

Therefore, the maximum upshift (seen in the laboratory frame) for an underdense ionization front will occur when  $\omega'_b = (\omega_c^2 + \omega_p^2)^{1/2}$ . We obtain this maximum upshifted frequency by substituting  $(\omega_c^2 + \omega_p^2)^{1/2}$  for  $\omega'_b$  in Eq. 2.2. Thus

$$\omega_b(max) = (\omega_c^2 + \omega_p^2)^{1/2} \gamma \left\{ 1 - \beta \left( 1 - \frac{\omega_c^2 + \omega_p^2}{\omega_c^2 + \omega_p^2} \right)^{1/2} \right\},$$

or

$$\omega_b(max) = \gamma (\omega_c^2 + \omega_p^2)^{1/2} = \left[ \frac{\omega_c^2 + \omega_p^2}{1 - \beta^2} \right]^{1/2} = \left[ \frac{\omega_c^2 + \omega_p^2}{1 - (v_{front}/c)^2} \right]^{1/2}.$$

Substituting  $v_{front}$  given by Eq. 2.1 we see that

$$\omega_b(max) = \omega_i \tag{2.12}$$

Thus the maximum upshifted frequency obtainable using underdense fronts is the frequency of the ionizing radiation [4]. At that frequency the upshifted radiation is propagating at the same velocity and in the same direction as the front (in the laboratory frame).

For densities above the critical density, the wave vector changes sign (the ball begins to roll back down the hill). This situation, where the wave is propagating through the density gradient in the same direction as the front (when viewed from the front's frame) is referred to as the co-propagating front scenario (see Fig. 2.3c). Although the frequency of the radiation is unchanged in this frame, the wave number is changing to continue to obey the dispersion relation which is a function of the plasma density. When we make a Lorentz transformation back

to the laboratory frame, this change in the wave number will manifest itself in a change in both the frequency and the wave number of the upshifted radiation [7, 8, 12].

If the interaction region is long enough, the reflected radiation will propagate completely down the density gradient (to the bottom of the hill). Once the wave has passed all the way back through the gradient, it is again in free space and is a truly reflected wave (see Fig. 2.3d). The upshift of such a reflected wave is a result of the relativistic Doppler effect [3]. This can be derived by Lorentz transforming to the front's frame, reversing the direction of the transformed wave vector, then Lorentz transforming back to the laboratory frame. For the waveguide case, this upshift is given by

$$\omega'_b(\text{refl}) = \omega \frac{(1 \mp 2\beta v_g/c + \beta^2)}{(1 - \beta^2)}. \quad (2.13)$$

If we again assume that this reflection takes place at the density where

$$\omega'_b = \omega \gamma (1 \mp \beta v_g/c) = (\omega_c^2 + \omega_p^2)^{1/2},$$

then  $\gamma (\omega_c^2 + \omega_p^2)^{1/2} = \omega_l$ , and we can write

$$\omega'_b(\text{refl}) = \omega_l \frac{(1 \mp 2\beta v_g/c + \beta^2)}{(1 \mp \beta v_g/c)}. \quad (2.14)$$

For relativistic fronts, where  $\beta \approx 1$ , this reduces to

$$\omega'_b(\text{refl}) = 2\omega_l \frac{(1 \mp v_g/c)}{(1 \mp v_g/c)} = 2\omega_l. \quad (2.15)$$

The upshifted frequency is plotted versus the plasma frequency of the front for three values of incident radiation frequency in Fig. 2.4. For our experimental parameters,  $\omega/\omega_l = 3 \times 10^{-5}$ . The solid curves which terminate at  $\omega_l$  are the underdense upshifts given by Eq. 2.2. The dashed curves which begin at  $2\omega_l$  [4] are



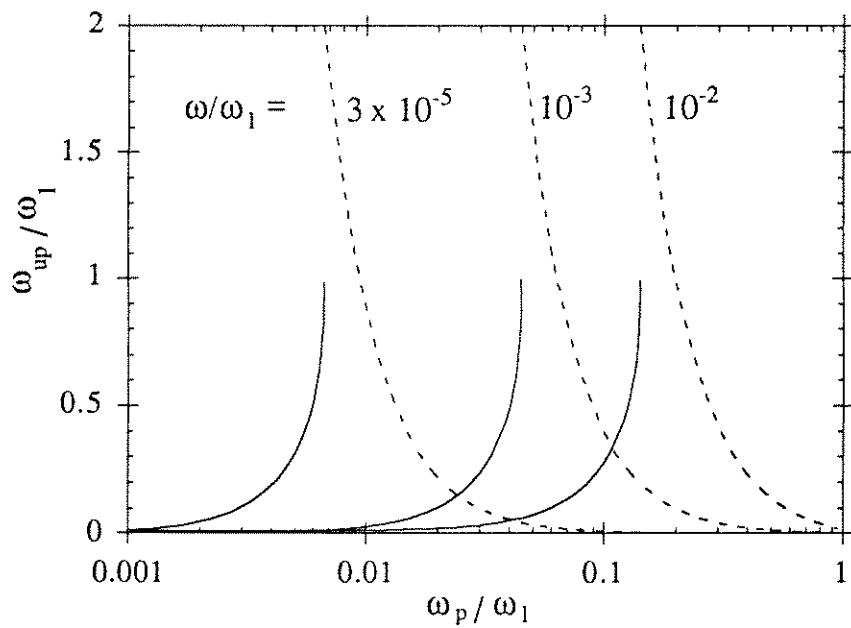


Figure 2.4: Upshifted frequency vs. plasma density of the front for three values of incident frequency. All frequencies are normalized to the ionizing laser frequency.  $3 \times 10^{-5}$  is the value for our experiments. The solid lines are the underdense upshifts and the dashed lines are the overdense reflected wave upshifts.

the reflected wave upshifts given by Eq. 2.13. They decrease at higher densities because they are strongly dependent on the front's velocity (see Eq. 2.1). For the reflected upshifts we have assumed that the interaction length is sufficient to allow the wave to travel all the way back through the density gradient. If the wave only traverses part of it, the upshift will be between  $\omega_l$  and  $2\omega_l$ .

## 2.4 Derivation of Reflection and Transmission Coefficients in Waveguide

The reflection and transmission coefficients for a TE wave polarized perpendicular to the plane of incidence (s-polarization) can easily be calculated in the front's frame (recall that in this frame the problem is reduced to that of a stationary boundary). We first derive the modes that can exist in the streaming plasma. The momentum equation for the electrons in the front's frame is

$$\frac{\partial \vec{v}}{\partial t} + \vec{U} \frac{\partial \vec{v}}{\partial z} = -\frac{e}{m_0 \gamma} (\vec{E} + \frac{1}{c} \vec{U} \times \vec{B}). \quad (2.16)$$

$\vec{U}$  is the velocity of the neutral gas, which in this frame is equal to the velocity of the front, and  $m_0$  is the rest mass of the electrons. We use two of Maxwell's equations,

$$\nabla \times \vec{E} = -\frac{1}{c} \frac{\partial \vec{B}}{\partial t} \quad (2.17)$$

and

$$\nabla \times \vec{B} = \frac{1}{c} \frac{\partial \vec{E}}{\partial t} - \frac{4\pi}{c} \vec{J}, \quad (2.18)$$

where  $\vec{J}$ , the free current, is  $ne\vec{v}$ . By taking the curl of Eq. 2.17, considering only TE waves ( $\nabla \cdot \vec{E} = 0$ ), and substituting the right side of Eq. 2.18 for  $\nabla \times \vec{B}$ , we

can write

$$\nabla^2 \vec{E} = \frac{1}{c^2} \frac{\partial^2 E}{\partial t^2} - \frac{4\pi n e}{c^2} \frac{\partial v}{\partial t}. \quad (2.19)$$

We Fourier analyze by assuming solutions of the form  $e^{i(\vec{k}\cdot\vec{r}-\omega t)}$ . Differentiating Eq. 2.19 gives

$$\left(\frac{\omega^2}{c^2} - k^2\right) \vec{E} = \frac{-i4\pi n e \omega}{c^2} \vec{v}. \quad (2.20)$$

We can now differentiate Eq. 2.16 and eliminate  $\vec{E}$  and  $\vec{B}$  using Eqs. 2.17 and 2.20 to write, after a bit of algebra,

$$(\omega - U k_{\parallel}) \left(1 - \frac{\omega_p^2}{\omega^2 - c^2 k^2}\right) = 0, \quad (2.21)$$

where the subscript  $\parallel$  denotes along the direction of  $U$ , which is opposite to the direction of propagation of the front. This equation has three roots,

$$k_{1\parallel} = \frac{\omega}{U}, \quad (2.22)$$

$$k_2 = \frac{\omega}{c} \left(1 - \frac{\omega_p^2}{\omega^2}\right)^{\frac{1}{2}}, \quad (2.23)$$

and

$$k_3 = -\frac{\omega}{c} \left(1 - \frac{\omega_p^2}{\omega^2}\right)^{\frac{1}{2}}. \quad (2.24)$$

We neglect the third root because we assume a positive value for the wave number of the source wave.

Now that we know that there are two possible modes in the streaming plasma, we can apply the boundary conditions to solve for the reflection and transmission coefficients. We assume a discontinuous boundary between the neutral gas and the plasma, which lies in the x-y plane.  $U$  is along the z axis and an electromagnetic wave with its electric field along the x axis is incident upon the boundary

with its wave vector in the y-z plane (s-polarization). Three independent conditions that must be satisfied at the plasma-neutral boundary are: 1) continuity of the tangential component of  $\vec{E}$ , 2) continuity of the normal component of  $\vec{B}$ , and 3) the total current must be zero because the electrons and ions have identical initial velocities when they are created at the boundary. Considering an incident mode (subscript  $i$ ), a reflected mode (subscript  $r$ ), and the two transmitted modes derived earlier (subscripts 1 and 2) these boundary conditions can be written as:

$$\left(\vec{E}_i + \vec{E}_r\right)_\perp = \left(\vec{E}_1 + \vec{E}_2\right)_\perp \quad (2.25)$$

$$\left(\vec{B}_i + \vec{B}_r\right)_\parallel = \left(\vec{B}_1 + \vec{B}_2\right)_\parallel \quad (2.26)$$

and

$$\nabla \times (\vec{B}_1 + \vec{B}_2) = \frac{1}{c} \frac{\partial}{\partial t} (\vec{E}_1 + \vec{E}_2). \quad (2.27)$$

In our geometry, Eqs. 2.25 and 2.26 become

$$E_i + E_r = E_1 + E_2 \quad (2.28)$$

and

$$B_i \frac{k_{i\parallel}}{k_i} - B_r \frac{k_{r\parallel}}{k_r} = B_1 \frac{k_{1\parallel}}{k_1} - B_2 \frac{k_{2\parallel}}{k_2}. \quad (2.29)$$

Realizing that  $B = (ck/\omega)E$  for each mode and that  $k_{i\parallel} = k_{r\parallel}$ , we can eliminate the reflected mode from the two equations above and write

$$E_1 = \frac{2E_i - E_2 \left(1 + \frac{k_{2\parallel}}{k_{i\parallel}}\right)}{\left(1 + \frac{k_{1\parallel}}{k_{i\parallel}}\right)} \quad (2.30)$$

Eq. 2.27 can be differentiated and rearranged to give

$$E_1 = E_2 \left( \frac{\omega^2 - c^2 k_2^2}{c^2 k_1^2 - \omega^2} \right). \quad (2.31)$$

We can now equate Eqs. 2.30 and 2.31 and reduce them to

$$\frac{E_2}{E_i} = \frac{2}{\left(1 + \frac{k_{2\parallel}}{k_{i\parallel}}\right) + \left(1 + \frac{k_{1\parallel}}{k_{i\parallel}}\right) \left(\frac{\omega^2 - c^2 k_2^2}{c^2 k_1^2 - \omega^2}\right)}. \quad (2.32)$$

Using this and Eq. 2.31, we obtain

$$\frac{E_1}{E_i} = \frac{2}{\left(1 + \frac{k_{1\parallel}}{k_{i\parallel}}\right) + \left(1 + \frac{k_{2\parallel}}{k_{i\parallel}}\right) \left(\frac{c^2 k_1^2 - \omega^2}{\omega^2 - c^2 k_2^2}\right)}. \quad (2.33)$$

And finally, Eq. 2.28 simply gives us

$$\frac{E_r}{E_i} = \frac{E_1}{E_i} + \frac{E_2}{E_i} - 1. \quad (2.34)$$

Thus Eqs. 2.32, 2.33, and 2.34 give us the reflection and transmission coefficients in the front's frame. In order to obtain the laboratory frame coefficients, we must transform back to the laboratory frame.

We make the Lorentz transformation using the relations

$$\vec{E}_{lab} = \gamma(\vec{E} + \vec{\beta} \times \vec{B}) - \frac{\gamma^2}{\gamma + 1} \vec{\beta}(\vec{\beta} \cdot \vec{E}) \quad (2.35)$$

and

$$\vec{B}_{lab} = \gamma(\vec{B} + \vec{\beta} \times \vec{E}) - \frac{\gamma^2}{\gamma + 1} \vec{\beta}(\vec{\beta} \cdot \vec{B}). \quad (2.36)$$

Using these relations, we can write the electric fields in the laboratory frame as

$$\vec{E}_{ilab} = \vec{E}_i \gamma \left(1 - \beta \frac{k_{i\parallel} c}{\omega}\right), \quad (2.37)$$

$$\vec{E}_{rlab} = \vec{E}_r \gamma \left(1 + \beta \frac{k_{i\parallel} c}{\omega}\right), \quad (2.38)$$

$$\vec{E}_{1lab} = 0, \quad (2.39)$$

and

$$\vec{E}_{2lab} = \vec{E}_2 \gamma \left(1 - \beta \frac{k_{2\parallel} c}{\omega}\right). \quad (2.40)$$

Because  $\vec{E}_1$  transforms to zero in the laboratory frame, we see that this mode is simply a static magnetic field. We can use the relation  $B_1 = (ck_{1\parallel}/\omega)E_1$  to obtain  $B_1$ , then transform back to the laboratory frame to give

$$\vec{B}_{1lab} = E_1\gamma \left\{ \left( \frac{ck_{1\parallel}}{\omega} - \beta \right) \hat{\perp} + \frac{ck_{1\perp}}{\gamma\omega} \hat{\parallel} \right\} \quad (2.41)$$

or

$$B_{1lab} = E_1\gamma \left\{ \left( \frac{ck_{1\parallel}}{\omega} - \beta \right)^2 + \left( \frac{ck_{1\perp}}{\gamma\omega} \right)^2 \right\}^{\frac{1}{2}}. \quad (2.42)$$

We can now write, after a considerable amount of algebraic manipulation, the laboratory frame reflection and transmission coefficients as

$$r \equiv \frac{E_{rlab}}{E_{ilab}} = \frac{(\sqrt{\epsilon'_i} - \sqrt{\epsilon'_t})}{(\sqrt{\epsilon'_i} + \sqrt{\epsilon'_t})}, \quad (2.43)$$

$$t_2 \equiv \frac{E_{2lab}}{E_{ilab}} = \frac{2\sqrt{\epsilon'_i}}{(\sqrt{\epsilon'_i} + \sqrt{\epsilon'_t})}, \quad (2.44)$$

and

$$t_1 \equiv \frac{B_{1lab}}{E_{ilab}} = \left\{ \frac{1 - \beta^2}{1 - \beta^2\epsilon'_i} \right\}^{\frac{1}{2}} 2\beta\sqrt{\epsilon'_i} \frac{(\sqrt{\epsilon'_i} - \sqrt{\epsilon'_t})}{1 - \beta\sqrt{\epsilon'_t}}. \quad (2.45)$$

Here  $\epsilon'_i \equiv 1 - \omega_c^2/\omega'^2$  and  $\epsilon'_t \equiv 1 - (\omega_c^2 + \omega_p^2)/\omega'^2$  with primed quantities specified in the front's frame.

For the range of plasma densities and  $\sqrt{\epsilon'_i}$  values used in our experiments,  $r \approx 0$  and  $t \approx 1$ . Note that Eqs. 2.43, 2.44, and 2.45 reduce to the free space expressions in the limit  $\epsilon'_i \rightarrow 1$  ( $\omega_c = 0$ ). Although the ratio of the transmitted to incident powers at the front is always expected to be nearly unity, for large upshifts most of the incident energy is left in the free-streaming mode's static  $B$  field as the transmitted wave's duration shortens. The above model assumes

that the ionization front is discontinuous. Similar results are obtained for finite length underdense fronts [4], except that the energy in the free-streaming mode is instead converted to thermal energy in the plasma, as is the case for finite length overdense fronts [3].

## 2.5 Derivation of upshifted Pulselengths in Waveguide

In deriving the expected duration of the upshifted radiation for a given interaction geometry, we first consider the group velocity of the upshifted radiation within the waveguide. The group velocity of the upshifted radiation in the plasma in the front's frame is given by

$$v'_{g,f,b} = \frac{d\omega'_{f,b}}{dk'_{f,b}} = c^2 \frac{k'_{f,b}}{\omega'_{f,b}}. \quad (2.46)$$

By transforming this velocity back to the laboratory frame, we obtain the group velocity of the upshifted radiation inside the plasma-filled waveguide in the laboratory frame,

$$v_{g,f,b} = \frac{v'_{g,f,b} + v_{front}}{1 + v'_{g,f,b} v_{front}/c^2}. \quad (2.47)$$

Eq. 2.47 is plotted in Fig. 2.5 as a function of front density for typical experimental parameters. The group velocity of the forward wave, which is always greater than that of the source radiation, increases as the plasma density in the front increases. On the other hand, the group velocity of the backward wave initially decreases as the front density increases. It goes to zero when the front density is such that

$$\omega_p^2 = \omega^2(1 + \beta v_g/c)^2 - \omega_c^2. \quad (2.48)$$

At this point the group velocity of the backward wave changes sign, then increases in the forward direction as the plasma density continues to increase.

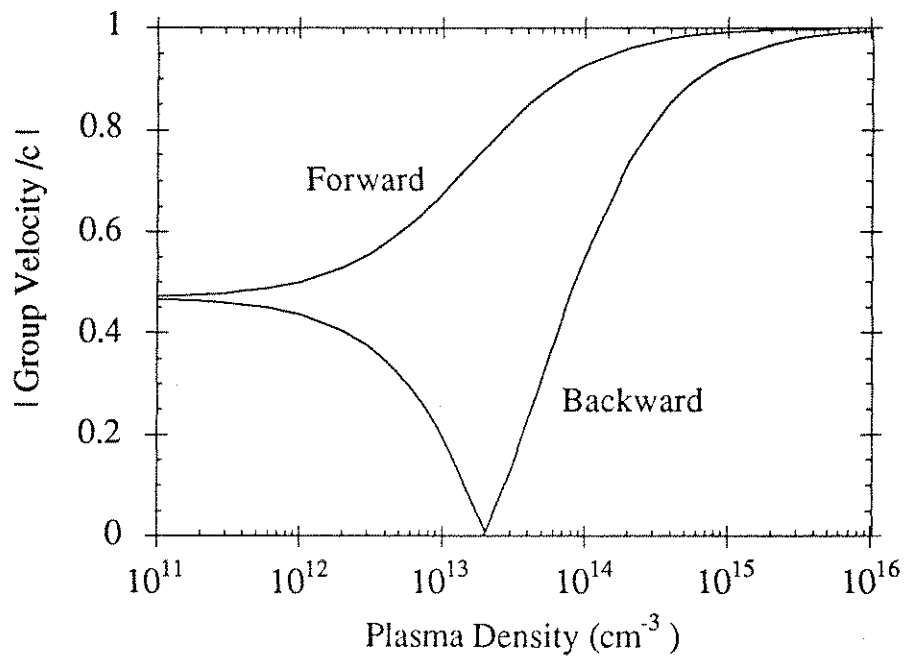


Figure 2.5: Group velocity of the *forward* and *backward* upshifted radiation vs. the plasma density in the front.



Once we know the group velocity of the upshifted radiation, we can easily determine the duration of the upshifted pulses. First consider the overtaken forward wave. For underdense fronts, the highest group velocity is that of the ionizing radiation. If we assume negligible depletion of the ionizing pulse or very short ionizing pulses, then the front will propagate at this same velocity. Thus the upshifted forward wave will begin to exit the waveguide at the instant the ionizing laser arrives at the laser output window (the forward window of the waveguide). The trailing edge of the forward upshifted pulse, which was generated at the instant the laser pulse entered the waveguide through the backward window and then propagated a distance  $x = v_{g_f}L/v_{front}$  before the forward wave began to leave the guide, will exit the waveguide after traveling the remaining  $L - x$  at  $v_{g_f}$ .  $L$  is the length of the waveguide. Similarly, for the backward wave, the pulse will begin to leave the waveguide at the instant the laser arrives at the backward window. The trailing edge of the backward pulse will leave the forward window, traveling toward the backward window, at the instant the laser pulse reaches the forward window. If the plasma density is high enough to turn the backward wave around, then the determination of its pulse length would follow the argument for the forward wave, but replacing  $v_{g_f}$  with  $v_{g_b}$ . Thus a general expression for the upshifted pulse lengths is

$$\tau_{pulse_{f,b}} = L \left| \frac{1}{v_{g_{f,b}}} - \frac{1}{v_{front}} \right|. \quad (2.49)$$

Eq. 2.49 is plotted for typical experimental parameters ( $L = 46$  cm, source  $v_g = .43 c$ ) in Fig. 2.6. The forward upshifted pulsewidth is  $\sim 2$  nsec for low plasma density and decreases dramatically at higher front densities. The pulsewidth of the upshifted backward wave starts at  $\sim 5$  nsec and initially increases, becoming

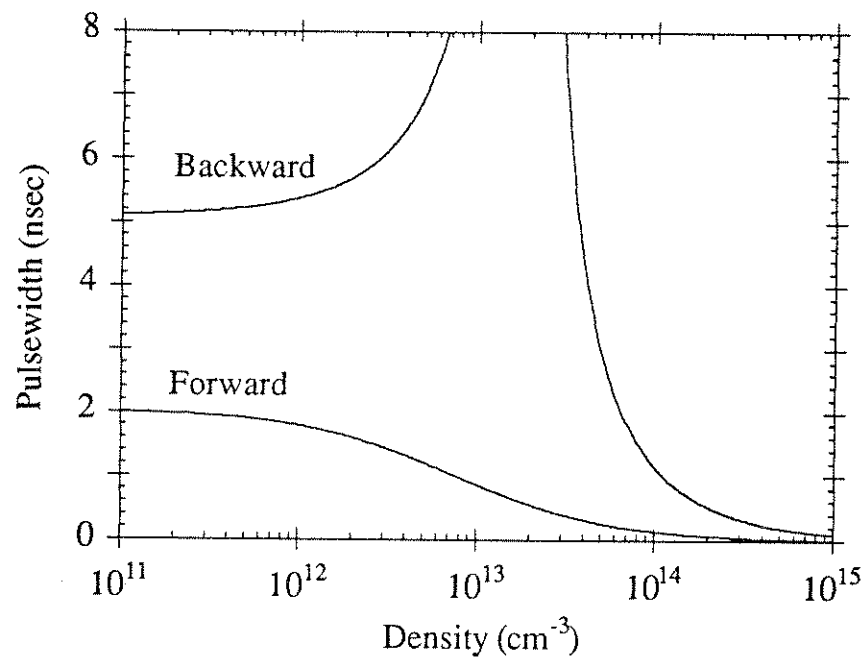


Figure 2.6: Expected upshifted pulse lengths vs. density for typical experimental parameters.

infinitely long as the wave approaches cutoff. At higher densities where the backward wave has turned around and attained a reasonably large group velocity in the forward direction, the pulsewidth is also significantly compressed.

## 2.6 “Reflection” of the *Backward Wave*

One of the most striking predictions of the underdense ionization front theory is the “reflection” of the backward wave. It is at first difficult to imagine that a wave propagating towards and transmitted through an approaching dielectric discontinuity will suddenly find itself propagating in the opposite direction. Consider a slab of plasma, or any other dielectric material, that is propagating through free space at a velocity,  $v_{slab}$ , toward an impinging electromagnetic wave [17]. Assume that the radiation is transmitted into the slab, as is the case for underdense ionization fronts. If the group velocity of the transmitted radiation inside the dielectric is greater than  $v_{slab}$ , then the radiation, which will have been upshifted in frequency at the moving boundary, will continue to propagate opposite to  $v_{slab}$  (at a slower velocity). When the upshifted radiation is transmitted through the other side of the slab (another moving boundary), its frequency and group velocity will return to their original values. Now consider what an observer would see if the group velocity of the upshifted radiation were less than  $v_{slab}$ . Although the radiation is transmitted into and propagates through the slab, the observer in the laboratory frame would see it traveling in the same direction (at a slower velocity) as the slab while it is inside. Because it has a slower velocity than the slab, it will eventually be overtaken and once it leaves the slab it would return to its original characteristics, as in the previous example.

Our ionization front experiments differ from the moving plasma slab examples.

The plasma itself is stationary, rather than moving at  $v_{slab}$ , and only the ionization boundary propagates at  $v_{front}$ . However, this has no effect on the upshifted frequencies or group velocities because the plasma frequency is Lorentz-invariant. Yet, because the recombination time of the plasma is long compared with the cavity transit times and the waveguide windows are stationary in the laboratory frame, the backward wave can turn around in the laboratory frame. When the upshifted group velocity is less than the front velocity, the observer will see the upshifted wave traveling through the plasma in the same direction as the front, as for the slab example. In the slab example the radiation then encountered the back edge of the slab and the group velocity returned to  $c$  in the backward direction. But in the ionization front case, the plasma recombination time is long and the second boundary encountered is the stationary cavity window (or plasma/neutral interface). Because the radiation was propagating toward this window while inside the plasma, it is transmitted through the window and propagates at  $c$  in the *forward* direction. The upshifted frequency and pulsewidth are very different from what would result from a true reflection from an overdense front or a moving mirror.

The space-time diagrams introduced in Sec. 2.2.2 are also useful for visualizing the backward wave turn-around. Fig. 2.7 is a space-time plot for a front density of  $1 \times 10^{13} \text{ cm}^{-3}$ , where the group velocity of the backward wave is small, but it is still propagating in the backward direction. The stippled area indicates source radiation that leaks out of the cavity before the arrival of the laser pulse. For a front density of  $4 \times 10^{13} \text{ cm}^{-3}$ , shown in Fig. 2.8, the backward wave has turned around and is propagating in the same direction as the ionizing laser. At this density the forward wave has already been significantly compressed in duration.

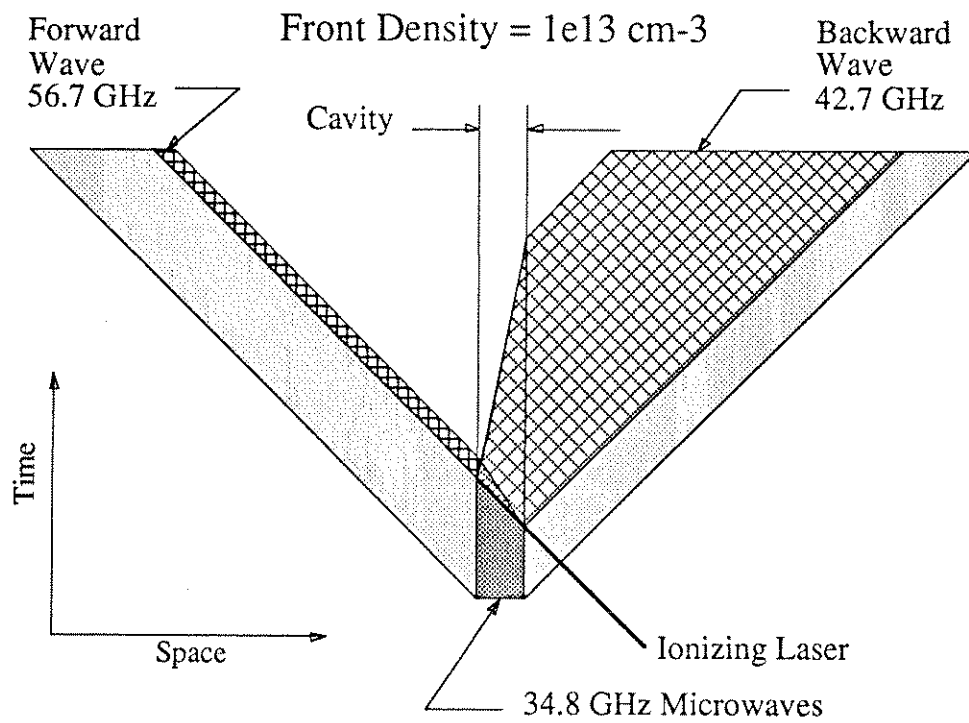


Figure 2.7: Space-time diagram for a front density of  $1 \times 10^{13} \text{ cm}^{-3}$ .

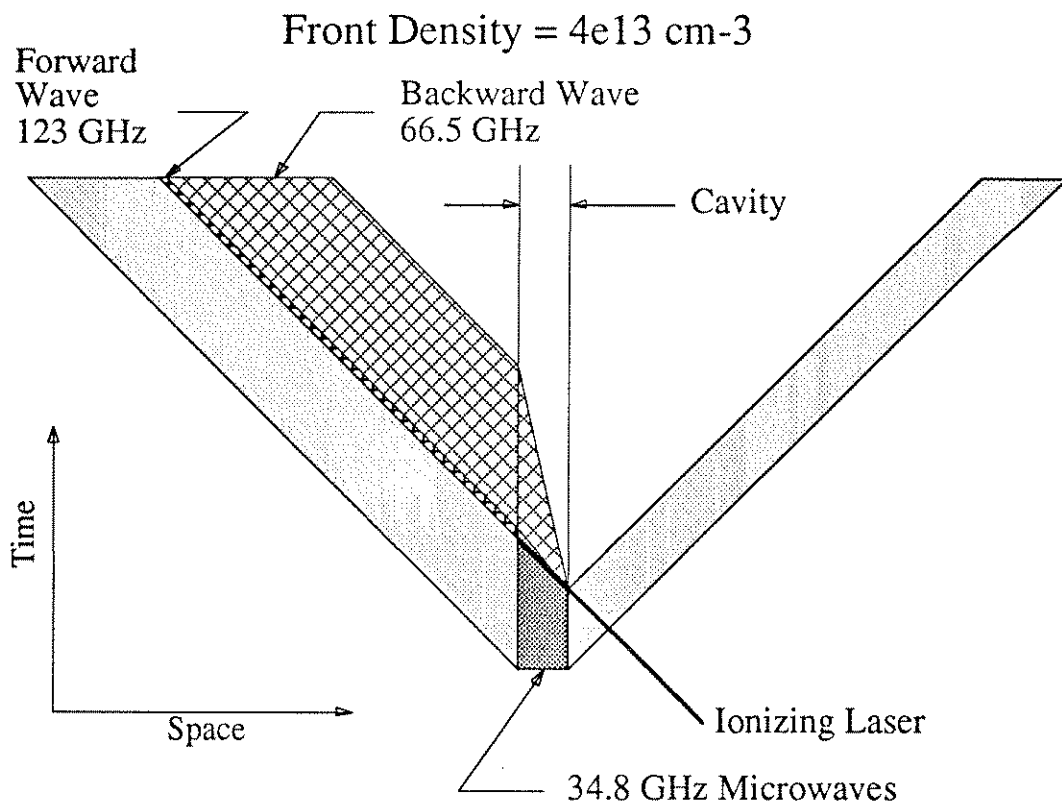


Figure 2.8: Space-time diagram for a front density of  $4 \times 10^{13} \text{ cm}^{-3}$ . At this density the upshifted *backward* wave is “reflected” into the *forward* direction.

Also, because the backward wave is now following along behind the front, its duration decreases significantly as its group velocity approaches that of the front at higher plasma densities.

## Chapter 3

### Experiment

Our experimental investigation of the interaction of underdense, relativistically-propagating ionization fronts has focused on two similar but distinct experimental configurations. Both utilize an ultraviolet laser pulse that ionizes a column of neutral gas enclosed by a waveguide. In both cases we investigate the interaction of 35 GHz microwave radiation which interacts with the front inside the waveguide.

The configuration that was used for the first experiments utilizes a resonant cylindrical waveguide cavity which is fed through the side wall. Because the cavity contains a standing microwave field, the front always interacts with a forward and a backward wave simultaneously. The experiments conducted with this cavity will be discussed in Section 3.1.

The second configuration utilizes a waveguide of rectangular cross-section which is fed along the axis via a directional coupler. In this case we are able to launch the microwave radiation in only either the forward or the backward direction. This allows us to better isolate the contributions of the two waves to our detected signals. We discuss the experiments conducted with this unidirectional configuration in Section 3.2.



### 3.1 Resonant Microwave Cavity Set-up

The experimental arrangement utilizing a resonant microwave cavity is shown schematically in Fig. 3.1. The cavity consists of a 1.2-cm-diameter, 35-cm-long

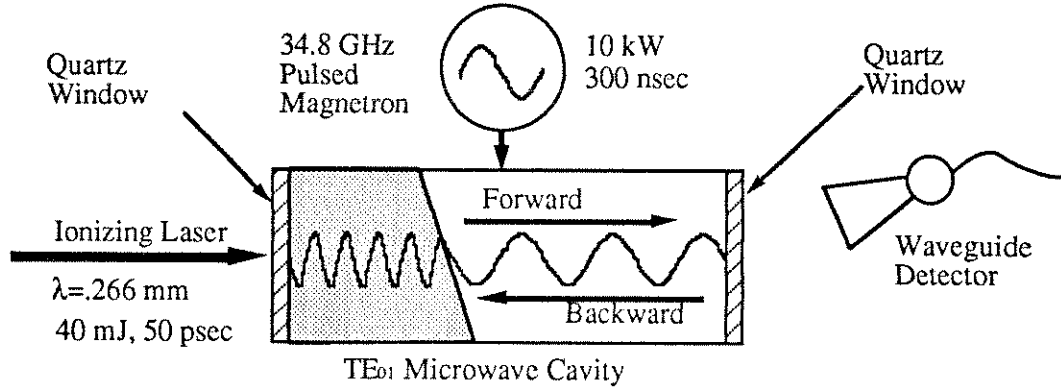


Figure 3.1: Schematic of the experimental arrangement utilizing a resonant microwave cavity.

copper cylinder that is closed by a 0.3-cm-thick quartz window at each end. Microwaves from a pulsed magnetron are fed into the cavity through the side wall at the mid-plane and excite the  $TE_{01}$  mode. The  $TE_{01}$  mode, sometimes referred to as the low-loss mode, has an azimuthal electric field inside the waveguide [16]. It was chosen because it is low-loss and it does not require a current to flow between the end plate (a quartz window in this case) and the cylindrical cavity wall in order to maintain a high  $Q$ . The measured  $Q$  of the cavity is  $\sim 1000$ . The magnetron gives a flat-top pulse with an instantaneous power of  $\sim 10$  kW and a duration of  $\sim 300$  nsec. The cavity is heated to 100 deg C in order to support azulene (which is solid at room temperature) vapor at pressures from a few to several hundred mT. Azulene is used because it is easily ionized by  $.266 \mu\text{m}$  radiation.

The ionizing laser pulse is derived from a mode-locked neodymium:yttrium

aluminum garnet (Nd:YAG) laser giving a train of 100-psec-long pulses at a wavelength of  $1.06 \mu\text{m}$ . Single pulses are selected from the train and amplified to the 200 mJ level in a Nd:YAG regenerative amplifier. These high-energy pulses are then frequency doubled twice using potassium titanium phosphate (KTP) crystals to give 50-psec-long (FWHM) pulses containing 40 mJ of energy at a wavelength of  $.266 \mu\text{m}$  in the ultraviolet. The output beam diameter is  $\sim 1$  cm and thus fills the cavity aperture. The laser system is capable of producing these amplified pulses at a repetition rate of 10 Hz. During experiments, the laser is typically fired once every 15 to 30 seconds in order to allow products of the ionization process to be pumped out of the waveguide.

Upshifted radiation is monitored by a series of diode detectors, each preceded by a length of rectangular waveguide and a horn, which are mounted at various positions at both ends of the cavity. To obtain sub-nanosecond resolution we use high-bandwidth SMA coaxial cables to transmit the signals to 1-GHz-bandwidth analog oscilloscopes (Tektronix 7104) which use a micro-channel plate to intensify the display. Terminating the signals into  $50 \Omega$  significantly reduces the sensitivity of the detectors, but gives high temporal resolution. The signals typically require attenuation of 30 to 40 dB in order to stay in the linear regime of the detector response. This is accomplished using a precision resistive-wafer-style variable attenuator mounted between the detector and the cutoff waveguide. The signals are recorded using digitizing CCD cameras mounted directly to the oscilloscope display. The digital images, captured via frame-grabber boards in a computer are then processed to extract the transient wave forms. These are then transported to an Apple Macintosh computer where they are scaled and further processed using National Instruments' LabView software. The bandwidth-limited temporal

resolution of our detection system is  $\sim 400$  psec (FWHM).

### 3.1.1 Frequency Measurements

A typical experimental run begins with the heated cavity evacuated to a base pressure of a few mT. Azulene vapor is then slowly introduced into the cavity through a precision leak valve. When the azulene pressure is low, the upshifted frequency of both the forward and backward waves is below the cutoff frequency of the detector waveguide and thus is not detected. Once the plasma inside the cavity is sufficiently dense to shift the waves above the detector cutoff, the signal rises sharply then decreases as the response of the detector rolls off with the higher frequencies that are generated at higher pressures. A typical upshifted wave form recorded on the 173 GHz detector channel is shown in Fig. 3.2. The early negative-going peak is a laser fiducial which triggers the oscilloscopes in synchronization with the ionizing laser pulse. For large upshifts (high azulene pressures) the upshifted signal is typically a single sub-nanosecond pulse, as shown.

In Fig. 3.3 we plot the onset of the upshifted signals measured in the forward direction for four detector channels at 40 GHz, 59 GHz, 91 GHz, and 116 GHz as a function of neutral gas pressure. The data points in the plot represent the amplitude of the peak in the signals. Because the cutoff response of the waveguide is extremely sharp (typically 40 to 60 dB over a few GHz), we interpret the sharp rise in signal amplitude as the point at which the radiation is upshifted to above the cutoff frequency. However, to compare the data with theoretical predictions, we must first determine the plasma density as a function of azulene pressure.

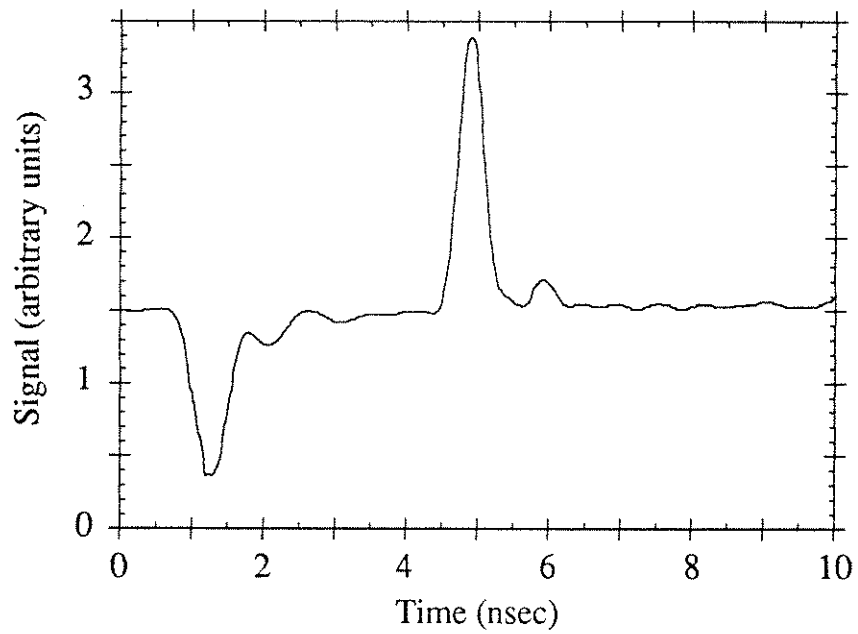


Figure 3.2: Typical upshifted signal using a 173 GHz cutoff waveguide. The negative-going peak is a laser fiducial.

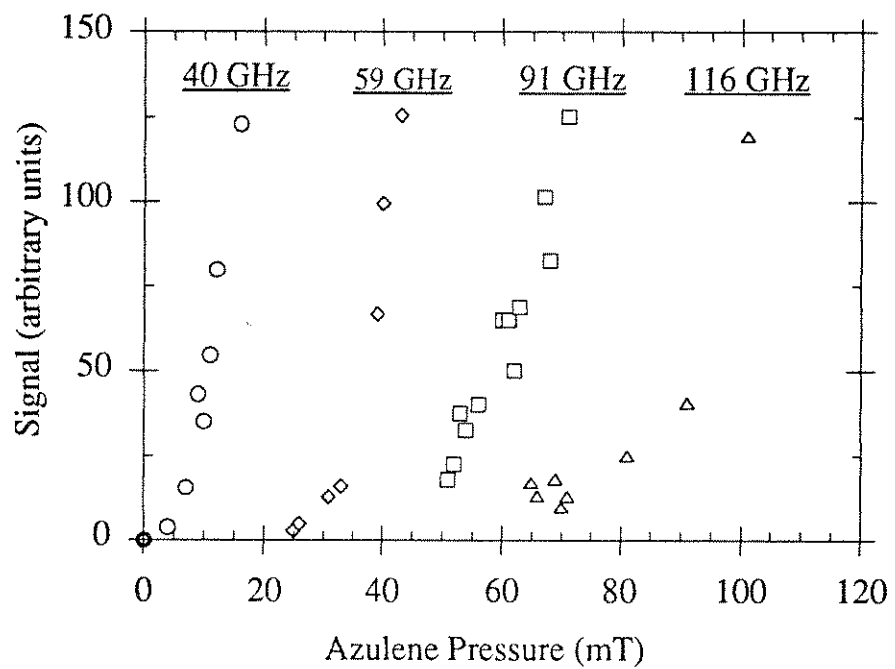


Figure 3.3: Onset of upshifted signals on the 40 GHz, 59 GHz, 91 GHz, and 116 GHz detector channels plotted vs. azulene pressure.

### 3.1.2 Interferometry Density Measurement

We have measured the plasma density with a 65 GHz microwave interferometer in a Michelson configuration. The plasma arm of the interferometer was defined by replacing the cavity window opposite the laser input with a Teflon window. Teflon was chosen because it reflects less than quartz at this wavelength. The interferometer's microwaves then entered the cavity through the Teflon window and the portion that reflected from the quartz window at the other end interfered with the reference beam in the interferometer. We thus measured the line-averaged plasma density. The interferometer was unable to temporally resolve the rapid creation of the plasma as the ionizing laser pulse traversed the cavity, but instead recorded the slower recombination of the plasma which occurs on a  $\mu\text{sec}$  time scale. A typical interferometer signal is shown in Fig. 3.4. As the laser pulse traverses the cavity the interferometer signal jumps to some initial level then unwinds back to its original value as the plasma recombines. Because the plasma decays exponentially in time, the fringes are progressively farther apart for later times. By counting the number of fringes, we are able to determine the density with a good degree of accuracy. The phase change due to the presence of the plasma is related to the plasma density by

$$\Delta\phi_{degrees} = \frac{360}{2\pi} L \left\{ \left[ \omega_{int}^2 - (\omega_c^2 + \omega_p^2) \right]^{1/2} - \left[ \omega_{int}^2 - \omega_c^2 \right]^{1/2} \right\}. \quad (3.1)$$

$L$  is the total length of the plasma sampled by the interferometer, twice the cavity length. The frequency of the radiation used to make the measurement is  $\omega_{int}$ , and  $\omega_c$  is the cutoff frequency of the mode of the interferometer radiation inside the cavity. The plasma density is determined from the plasma frequency,  $\omega_p$  using Eq. 1.1. The measured line-averaged plasma density is plotted as a function of

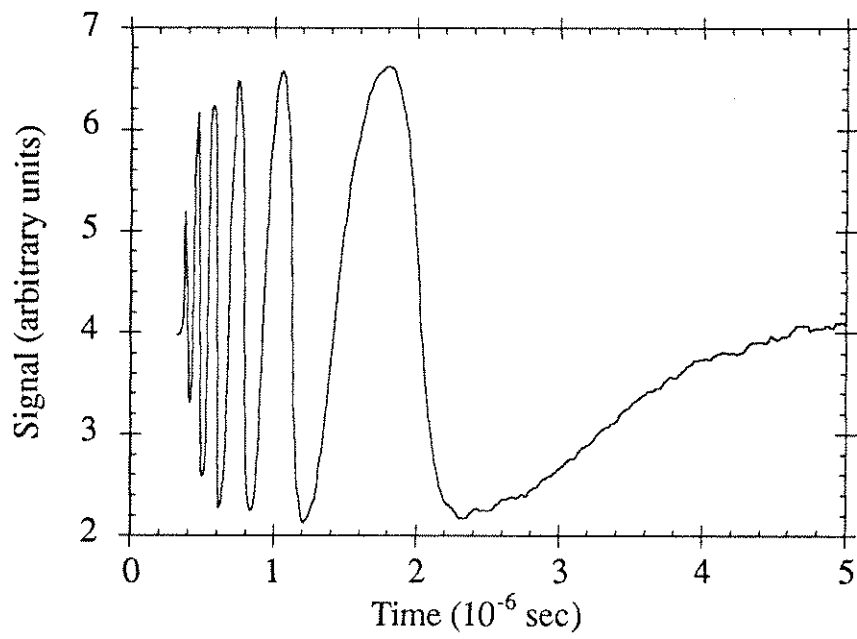


Figure 3.4: Typical signal from the 65 GHz interferometer.

azulene pressure up to 16 mT in Fig. 3.5. A least-squares fit to the data gives a

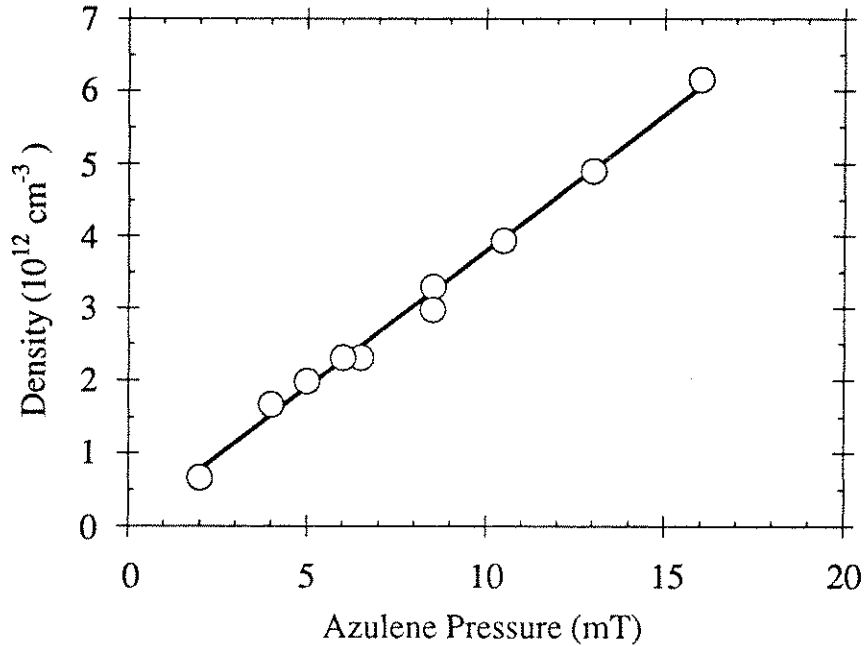


Figure 3.5: Measured plasma density plotted as a function of azulene pressure. The solid line is a least-squares fit.

conversion factor of  $\sim 3.8 \times 10^{11} \text{ cm}^{-3}$  per mT of azulene. This corresponds to a fractional ionization of  $\sim 1.5\%$  at 100 deg C.

### 3.1.3 Data Fit with Theory

With the conversion factor from azulene pressure to plasma density, the onset of the upshifted signals measured in the forward direction (see Fig. 3.3) can be plotted vs. front density as shown in Fig. 3.6. The horizontal bars represent the range of pressures over which the signals are sharply rising. The solid lines represent the theoretically predicted frequencies given by Eq. 2.2 for the forward



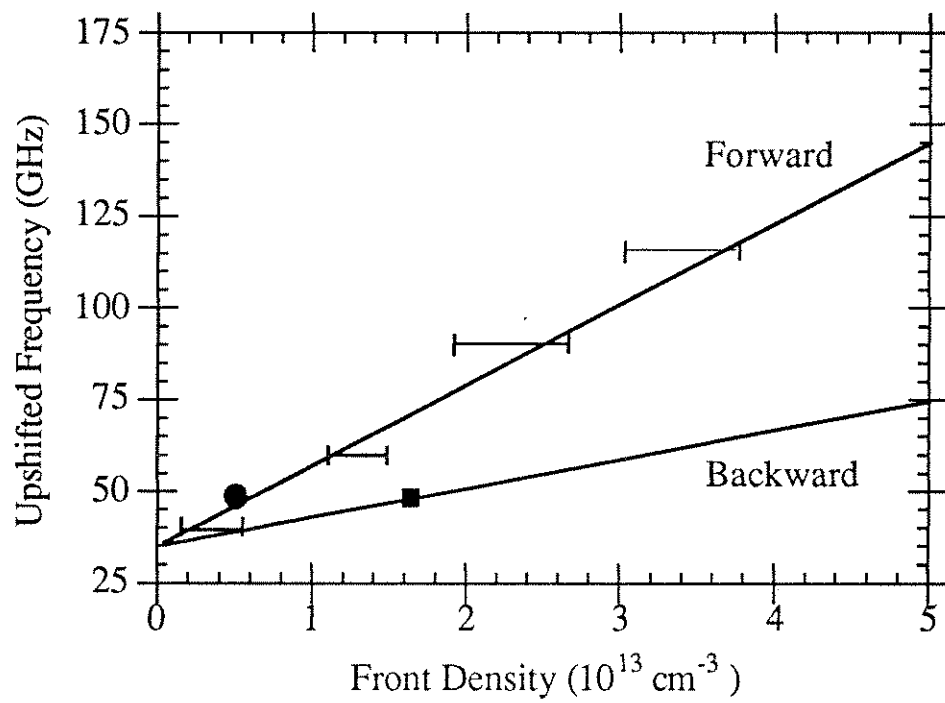


Figure 3.6: Experimentally detected upshifted signals plotted vs. the measured front density. The solid lines are the predictions of Eq. 2.2.

and backward waves. The data are in reasonable agreement with the predicted linear dependence of upshift on front density. Also, the degree of upshift is approximately what is expected for the forward wave.

### 3.1.4 Detection of the *Backward Wave*

The detection of the backward wave is complicated by several factors. As shown in Fig. 2.5, the group velocity of the backward wave, which is initially  $.47c$ , is significantly reduced over the whole range of plasma densities obtainable in these experiments. This causes an increase in the pulse length of the backward wave, thus reducing its power, which is what we detect. Also, when the backward wave is near cutoff, its transmission coefficient at the plasma/quartz boundary is small and the backward upshifted radiation is trapped in the cavity. The radiation detected in the backward direction has two sources: the backward wave and the forward propagating radiation that has reflected from the quartz output window into the backward direction. Because the upshifted backward wave begins to exit the cavity at the moment the ionizing laser pulse arrives, the reflected forward wave is delayed by the transit time of the laser pulse plus that of the forward radiation,  $\sim 2-3$  nsec. To identify the backward wave, we use a fast photo diode positioned near the entrance to the cavity to detect the arrival of the laser pulse and provide a time fiducial. We then record the temporal evolution of the radiation emitted in both the forward and backward directions as a function of azulene pressure.

Figures 3.7 and 3.8 show the signals detected in the forward and backward directions on the 48 GHz channel at an azulene pressure of 16 mT. Both signals exhibit a single sub-nanosecond peak and onset at approximately the same

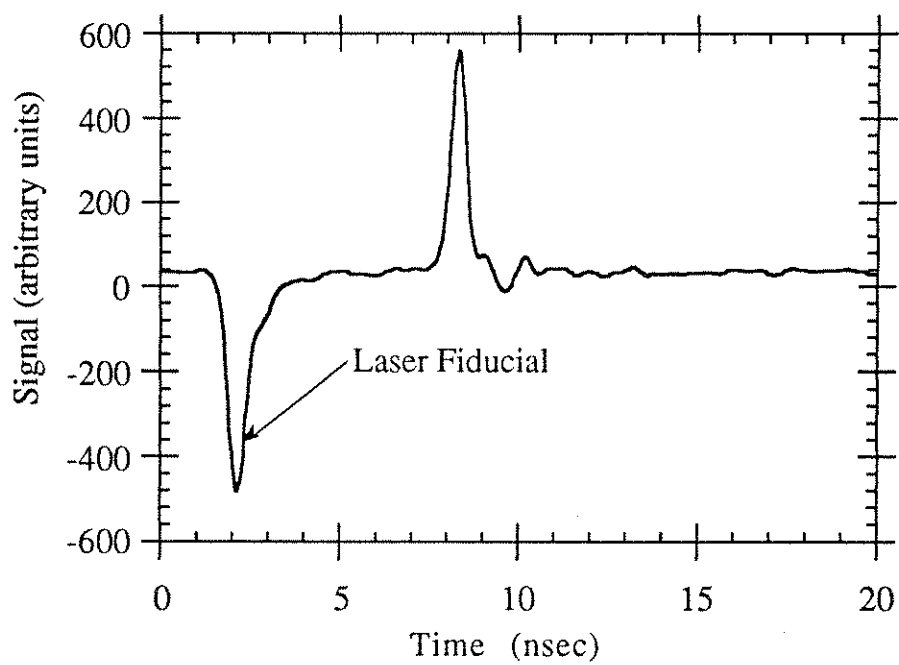


Figure 3.7: Upshifted signal measured in the forward direction on the 48 GHz detector channel at 16 mT azulene pressure.

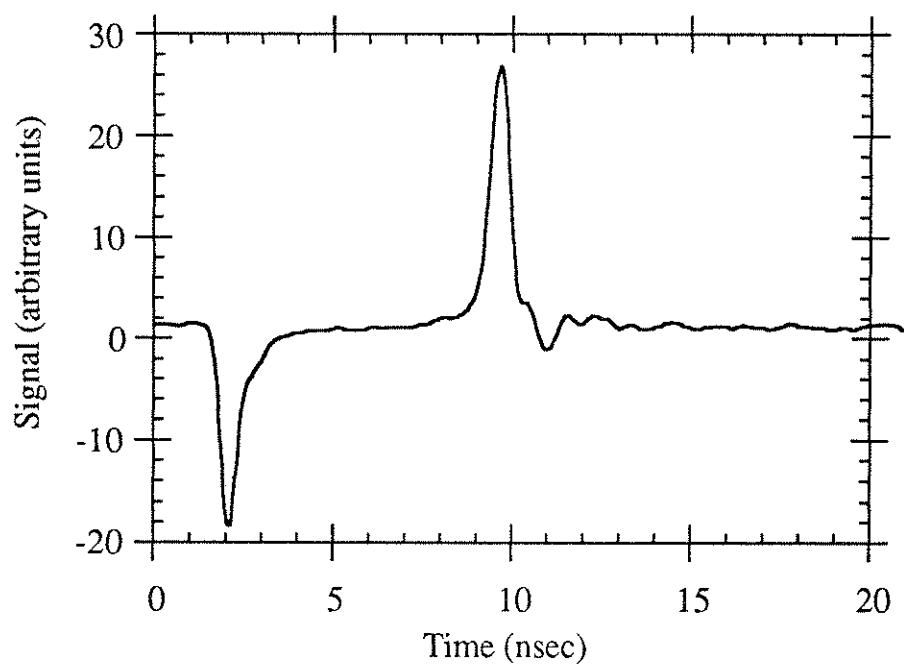


Figure 3.8: Upshifted signal measured in the backward direction on the 48 GHz detector channel at 16 mT azulene pressure.

pressure, which is plotted as the solid circle in Fig. 3.6. At this pressure, only the forward wave is expected to be upshifted above 48 GHz. We therefore interpret the backward signal as resulting from upshifted forward radiation that has reflected from the output window into the backward direction. Figure 3.9 shows the forward signal at 70 mT azulene pressure and Fig. 3.10 shows the

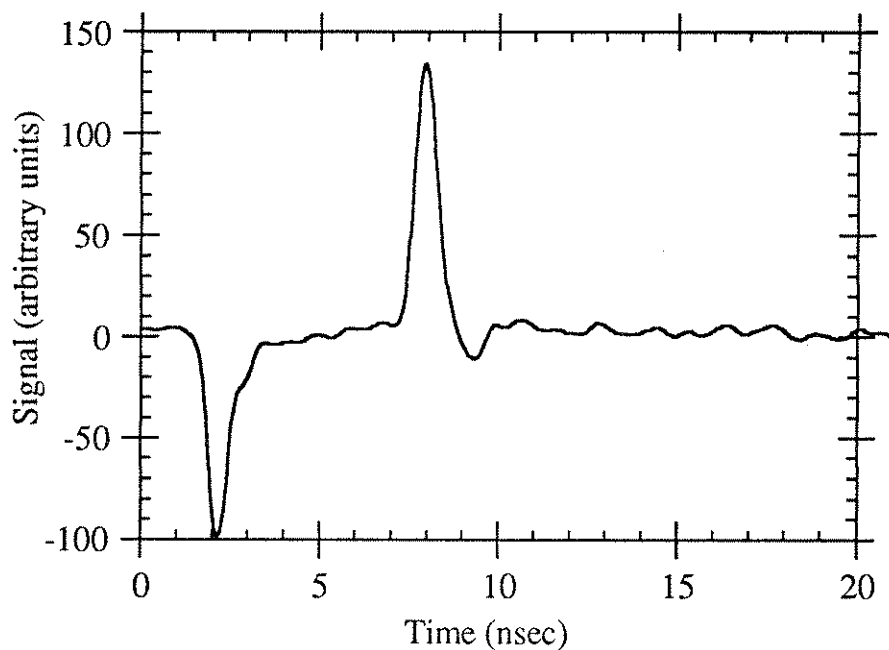


Figure 3.9: Upshifted signal measured in the forward direction on the 48 GHz detector channel at 71 mT azulene pressure.

backward signal at the same pressure. The forward signal continues to have only one peak, but a second earlier peak appears in the backward direction at higher pressures. The pressure at which this earlier peak onsets is shown by the solid square in Fig. 3.6. The onset occurs at approximately the predicted pressure for the backward wave to upshift to more than 48 GHz. This, together with

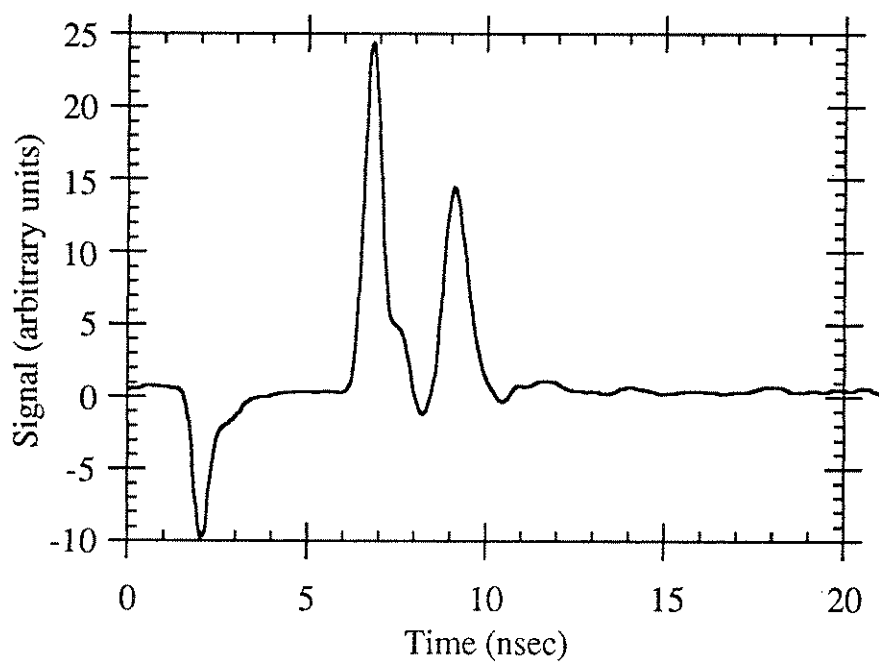


Figure 3.10: Upshifted signal measured in the backward direction on the 48 GHz detector channel at 71 mT azulene pressure.

the  $\sim 2.4$  nsec delay between the arrival of the two peaks, is consistent with identifying the earlier peak as the upshifted backward wave. However, Eq. 2.4 predicts that the backward wave reverses its propagation direction and exits the cavity in the forward direction when the front density is above  $2 \times 10^{13} \text{ cm}^{-3}$ . This turn-around density corresponds to an azulene pressure of  $\sim 50$  mT. Above this pressure, the forward and backward radiation are expected to arrive coincidentally at the forward detector. Therefore, with our present diagnostics, we are unable to differentiate between the two waves in the forward direction. That the peak associated with the backward wave persists in the backward direction at higher pressures is an issue that is investigated further as described in Sec. 3.2.

### 3.1.5 Efficiency

As discussed in Section 2.4, we expect the power conversion efficiency from the source wave to the upshifted wave to be 100 percent. Remember that this does not imply that the energy conversion efficiency is also 100 percent because the upshifted pulse may be compressed in duration. To obtain an estimate of the power conversion efficiency, we measure the antenna pattern of the upshifted radiation in one plane (parallel to the surface of the optical table) then, assuming the output is cylindrically symmetric, integrate azimuthally to obtain the total upshifted power. As shown in Fig. 3.11, the “butterfly” antenna pattern of the  $\text{TE}_{01}$  mode is preserved for upshifts close to the source frequency (40 GHz channel), but becomes peaked on axis as the degree of upshift increases, as shown in Fig. 3.12 for the 91 GHz channel. When the laser is blocked, the total radiated power at the source frequency is approximately 5.8 kW. The total upshifted power in the forward direction at 40 GHz is approximately 3.1 kW. If we define the upshifted

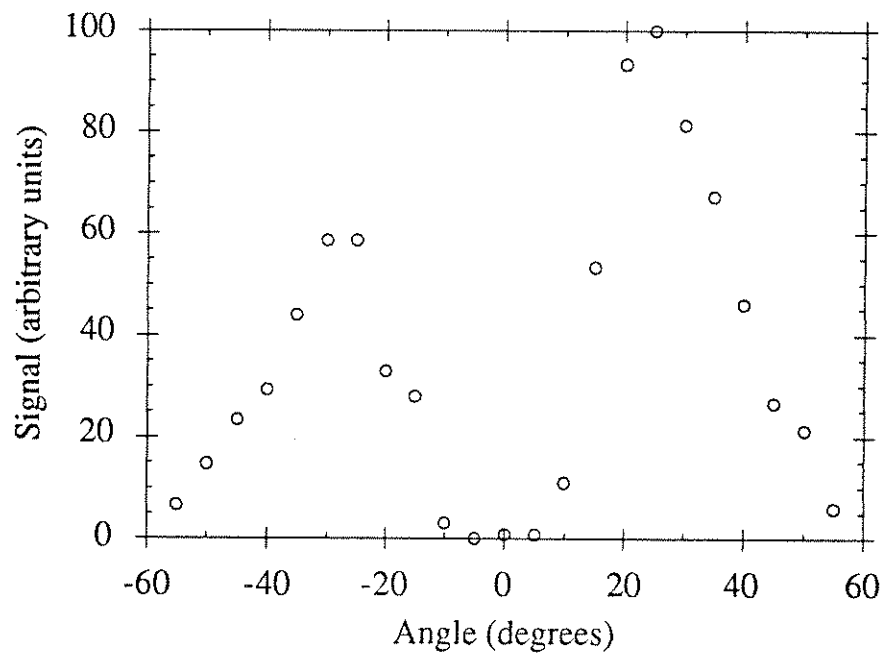


Figure 3.11: Antenna pattern of the upshifted radiation measured on the 40 GHz detector channel.



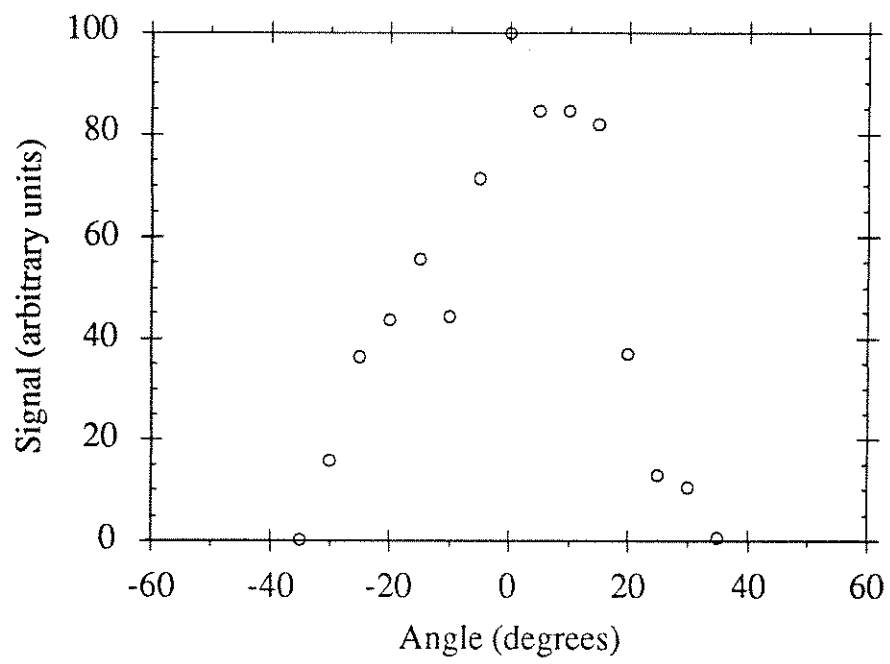


Figure 3.12: Antenna pattern of the upshifted radiation measured on the 91 GHz detector channel.

power efficiency as upshifted power radiated in the forward direction divided by the source power radiated in the forward direction with the laser blocked, the efficiency is greater than 50 percent at 40 GHz. Thus defined, the efficiency is only a fraction of a percent at 90 GHz where the forward radiated power is approximately 22 W. This lower efficiency may be largely due to laser pump depletion along the cavity axis causing the length over which a sufficiently dense front is created to decrease. This would reduce the duration of the upshifted pulses, possibly to the point where the detector response is severely bandwidth limited. Also, we expect the response of our detection system to be significantly reduced for large upshifts where the pulsewidths are expected to be much less than 1 nsec.

### **3.2 Unidirectional Microwave Cavity Set-up**

In order to investigate the role of the forward and backward waves independently, we conducted a series of experiments utilizing a unidirectional waveguide configuration. This experimental arrangement is shown schematically in Fig. 3.13. Microwave radiation is fed into a straight section of WR-19 waveguide through a 3 dB directional coupler (1:1 power divider). The waveguide is sealed at each end with a 0.1 mm-thick quartz window, chosen to be much less than a wavelength thick to reduce reflection. The measured ratio of the transmitted power to the reflected power is more than 10:1. The interaction waveguide consists of either one, two or three six-inch-long sections of WR-19 waveguide. It is heated, evacuated, and filled with azulene vapor as with the resonant cavity described in Sec. 3.1. The microwave source and the ionizing laser are also the same as those used in the previous experiments.

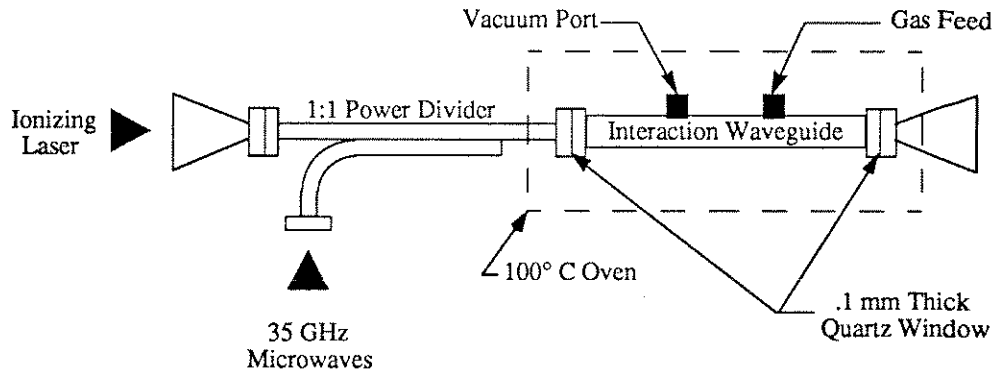


Figure 3.13: Schematic of the experimental arrangement utilizing a unidirectional cavity.

In the configuration shown in Fig. 3.13 we isolate the forward wave by launching the microwaves in the same direction as the ionizing laser. By either moving the directional coupler to the other side of the waveguide or directing the laser to enter from the other side, we are able to examine the backward wave interaction. Although we are able to launch a wave in predominantly the forward or backward direction, the upshifted radiation will leave the waveguide through a plasma/air interface. The reflections from this interface may be considerable, and we therefore expect upshifted signals to emanate from both ends of the cavity. Furthermore, small reflections from the thin quartz output window will give a small counter-propagating component to the launched wave. This may confuse the interpretation of the data when examining low amplitude upshifted signals. An additional benefit of the unidirectional waveguide over the resonant cavity is that the output is linearly polarized. This allows us to more easily utilize a diffraction grating to measure the upshifted spectra.

### 3.2.1 Grating Measurements

In previous experiments we used cutoff waveguides, acting as high-pass filters, to estimate the frequency of the upshifted radiation. This type of detection has the disadvantage that it gives little information about the spectral content of the upshifted pulse. It only senses that there is some radiation at frequencies above the cutoff frequency of the waveguide. In order to measure the spectrum of the upshifted radiation, we utilized a blazed diffraction grating with a period of 6.64 mm. The grating is simply a rectangular aluminum slab with grooves milled into the surface. The blaze angle is 30 degrees. The grating was placed approximately 2 m from the cavity output in the forward direction on a stage that allowed rotation about the surface of the grating as shown in Fig. 3.14. The angle between the incident radiation and the detected, diffracted beam was

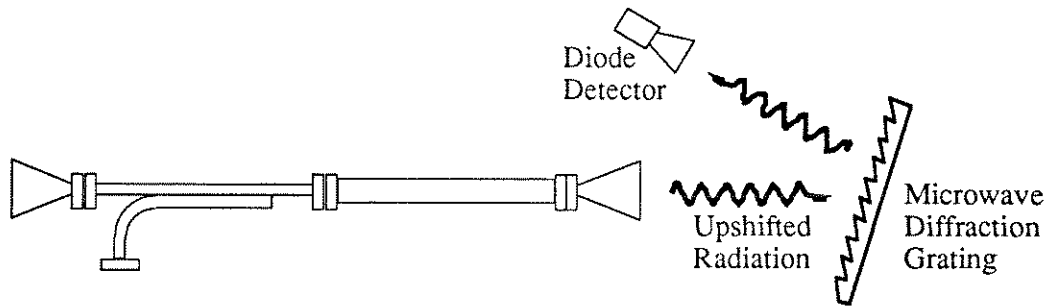


Figure 3.14: Schematic of the experimental arrangement utilizing a diffraction grating for frequency measurements.

chosen to be 10 degrees. This corresponds to the maximum efficiency angle for 40 GHz radiation. This angle can be varied so that the detector is always at the maximum efficiency angle for the detected frequency.

## Upshifted Spectra

With the detector fixed at the 10 degree position, we measured the spectrum of the forward upshifted radiation at several azulene pressures. These spectra are shown in Fig. 3.15. The resolution of our microwave spectrometer is shown by the

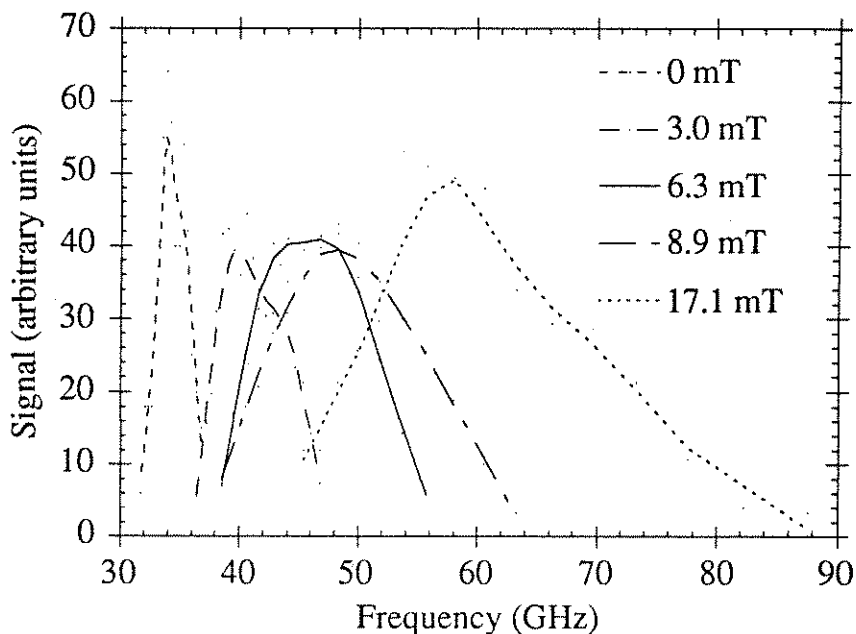


Figure 3.15: Spectra of forward-propagating upshifted radiation plotted vs. azulene pressure.

detected width of the source radiation to be  $\sim 2.5$  GHz. Although the detector angle was fixed, rather than optimized to maintain the detector at the maximum efficiency angle, it is readily seen in Fig. 3.15 that the spectra are peaked away from the source frequency. The center frequency increases with azulene pressure, as does the width of the spectra. A more detailed, optimized measurement at an azulene pressure of 5.5 mT is shown in Fig. 3.16. The upshifted spectrum is

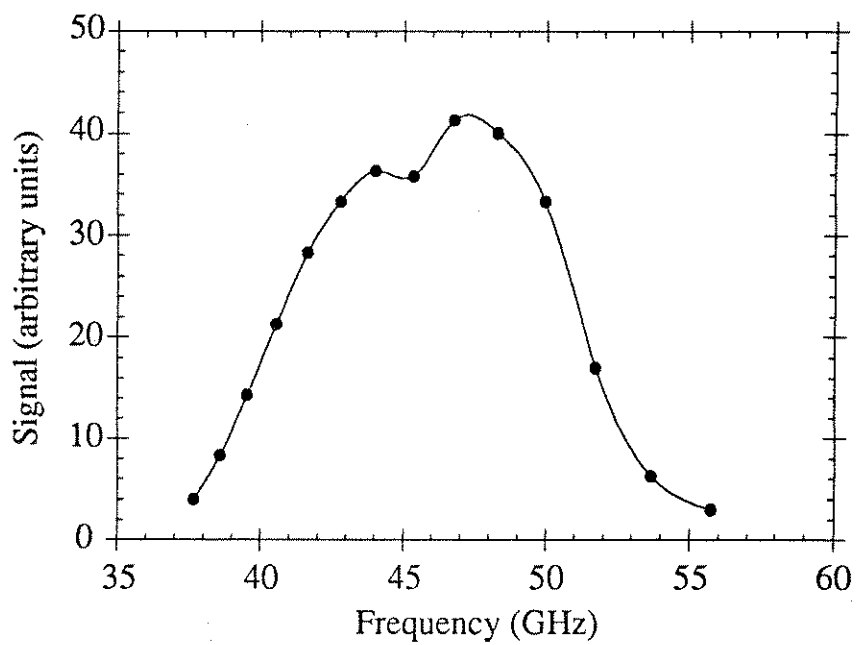


Figure 3.16: Optimized upshifted spectrum at 5.5 mT azulene pressure. The center frequency is 46 GHz.

peaked at  $\sim 46$  GHz and has a width of  $\sim 10$  GHz (FWHM) without accounting for the instrument function of our microwave spectrometer.

### Upshifted Frequencies

We again measured the plasma density using a 65 GHz microwave interferometer (see Sec. 3.1.2). In this configuration we were able to simply send the 65 GHz radiation into the coupling arm of the directional coupler (the same port through which the source microwaves usually enter). We placed a mirror at the output of the waveguide to reflect the microwaves back into the interferometer. A thin mica disk was taped to the center of the mirror to absorb the residual ionizing laser so that it did not make another pass through the cavity (which would cause further ionization). The measured plasma density is plotted as a function of azulene pressure in Fig. 3.17. From this measurement we obtain a conversion factor of  $\sim 9 \times 10^{11}$  cm<sup>-3</sup>/mT of azulene. With the density measured as a function of azulene pressure, we are able to compare the upshifted frequencies with theory. This is shown in Fig. 3.18 where the error bars indicate the width (FWHM) of the upshifted spectra. These are in reasonable agreement with the theoretical predictions, and the accuracy should be able to be improved by optimizing the detector position as described earlier.

### 3.2.2 Pulsewidth Measurement

The expected pulsewidths of the pulses of upshifted radiation were derived in Sec. 2.5 and plotted as a function of front density in Fig. 2.6. We measured the duration of the upshifted backward wave by positioning a detector preceded by a custom-made waveguide with a cutoff frequency of 36 GHz in the backward

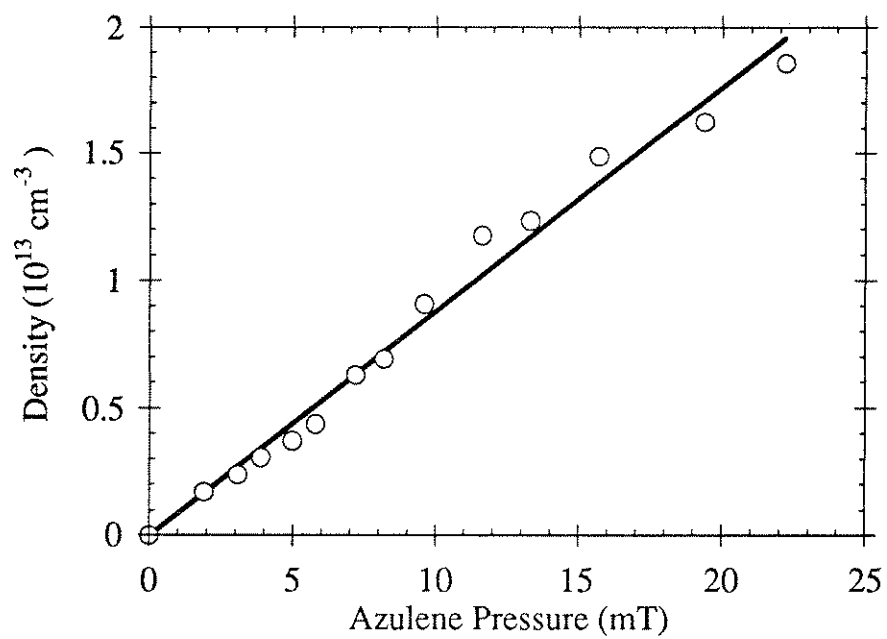


Figure 3.17: Plasma density measured with 65 GHz interferometer vs. azulene pressure. The conversion factor is  $\sim 9 \times 10^{11} \text{ cm}^{-3}/\text{mT}$ .



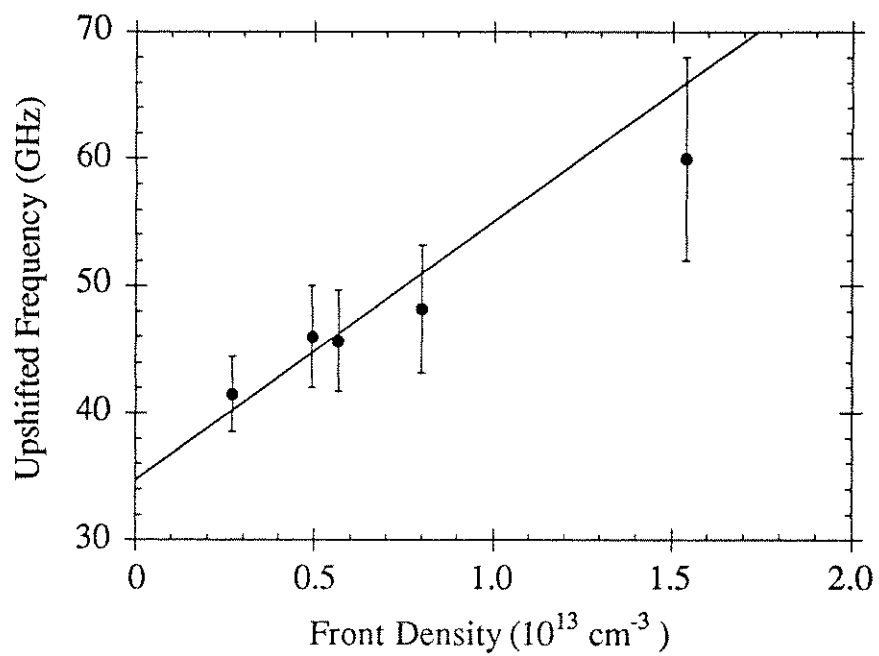


Figure 3.18: Center frequency of upshifted spectra plotted vs. azulene pressure. The solid line is the theoretical prediction. The error bars indicate the width (FWHM) of the upshifted spectra.

direction. The cutoff frequency of this detector is close to the source frequency so that we can detect small upshifts. The source frequency rejection is sufficiently high that we are unable to detect a signal from the source wave when we fire the magnetron with the ionizing laser blocked. Fig. 3.19 shows a backward upshifted

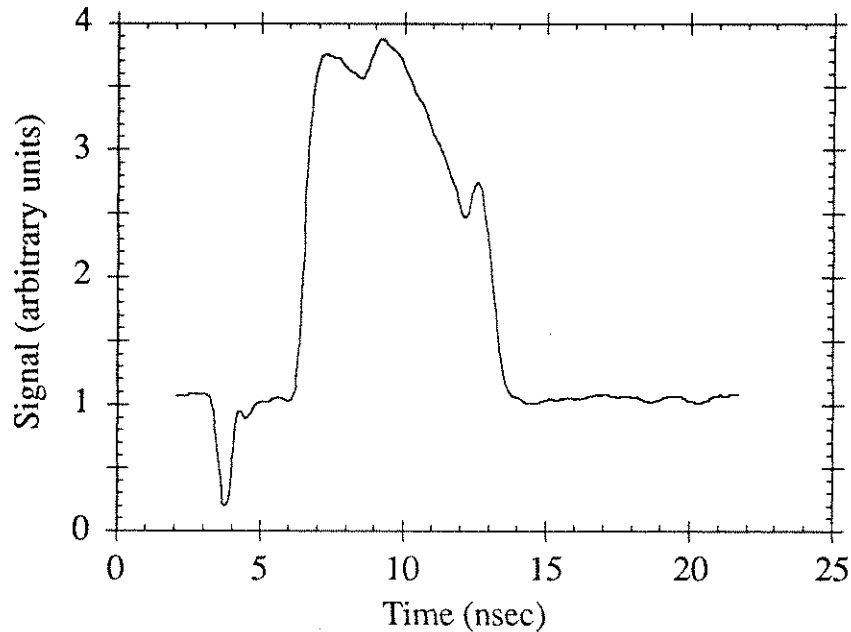


Figure 3.19: Backward upshifted signal recorded with a 36 GHz cutoff detector in the backward direction at 4 mT azulene pressure. The pulsewidth is  $\sim 7.5$  nsec.

signal recorded on the 36 GHz detector in the backward direction at an azulene pressure of 4 mT. The pulsewidth is  $\sim 7.5$  nsec. Fig. 3.20 is a similar signal taken with a 116 GHz cutoff detector in the forward direction while launching a forward wave. The pulsewidth is detection limited to  $\sim 0.5$  nsec.

In Fig. 3.21 we plot upshifted pulsewidths measured in the forward and back-

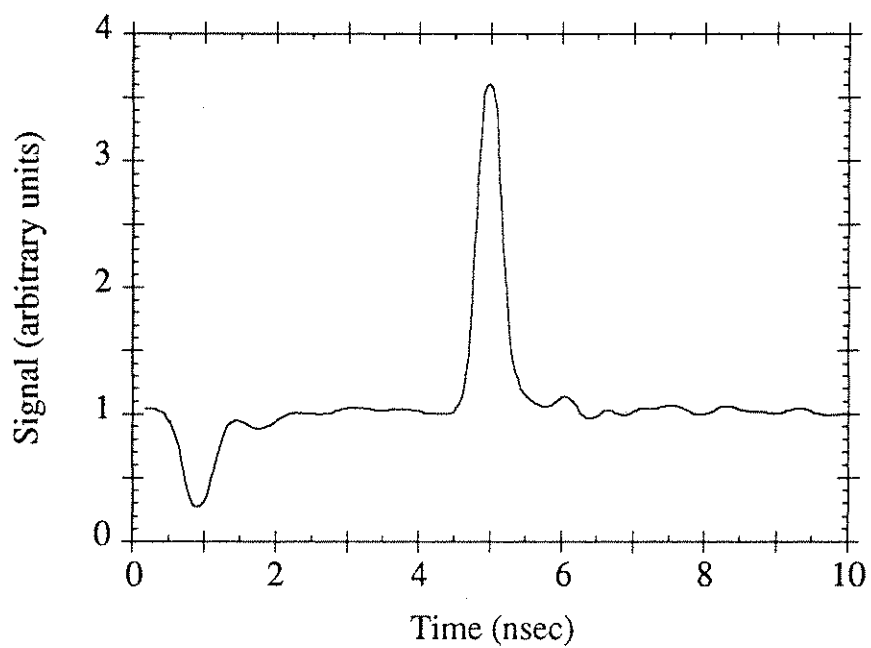


Figure 3.20: Forward upshifted signal recorded with a 116 GHz cutoff detector in the forward direction at 49 mT azulene pressure. The pulsewidth is detection limited to  $\sim 0.5$  nsec.

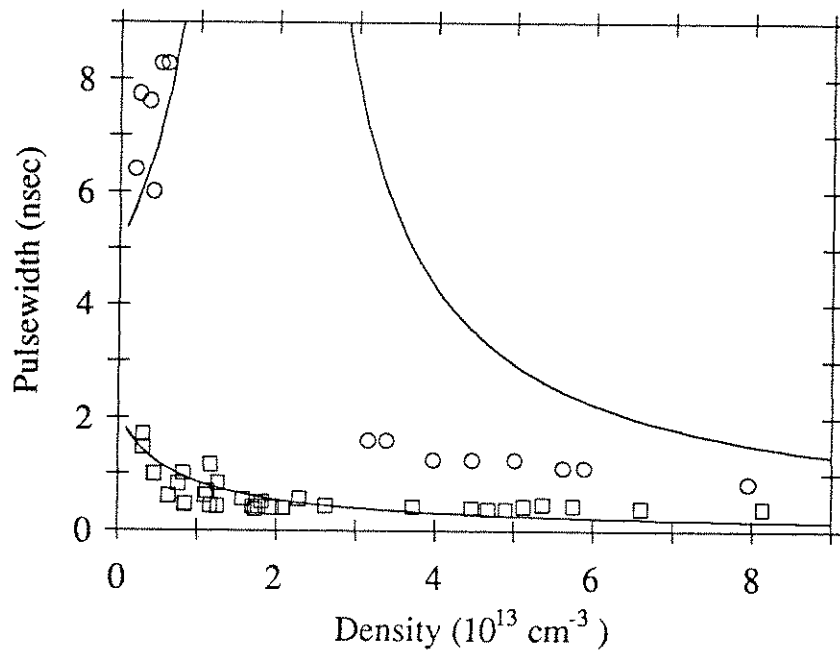


Figure 3.21: Measured upshifted pulsewidths of the forward (open squares) and backward (open circles) plotted vs. the front density. The solid curves are the theoretical predictions of Eq. 2.49

ward directions as a function of plasma density. The solid curves are the predictions of Eq. 2.49. At low azulene pressures, 2-8 mT, the backward signals are flat-top and long, 7-8 nsec, as expected. At pressures above  $\sim 10$  mT, the trailing edges of the flat-top pulses begin to erode, leaving a narrow peak at the leading edge of the pulse. Fig. 3.22 shows a partially eroded backward pulse at 10 mT

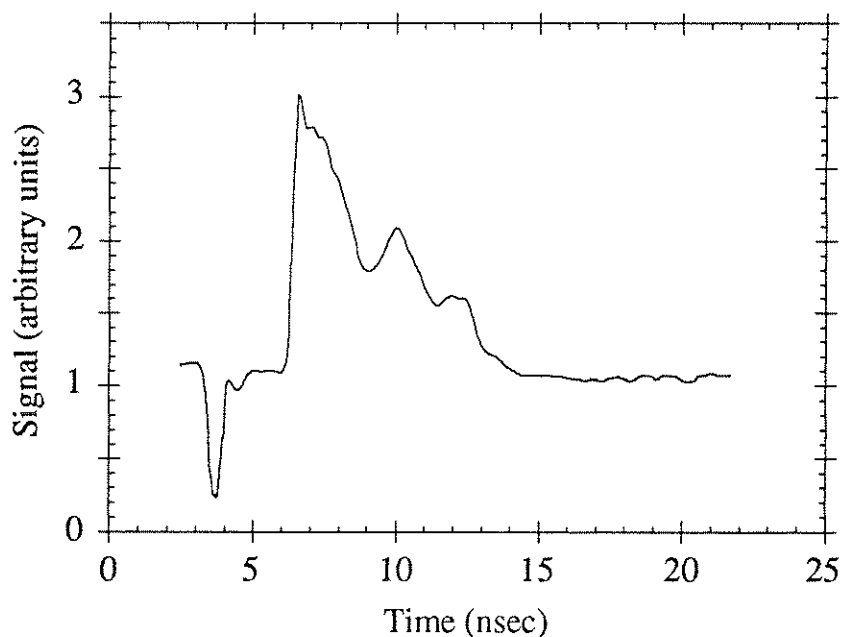


Figure 3.22: Backward upshifted signal recorded with a 36 GHz cutoff detector in the backward direction at 10 mT azulene pressure. The trailing edge of the pulse is partially eroded at this pressure.

of azulene. At 16 mT the long flat-top pulse has almost completely decayed, leaving a 1-nsec peak at the leading edge (see Fig. 3.23). This decay may be a manifestation of the group velocity of the upshifted backward wave approaching zero as it nears cutoff. At higher pressures, because we expected the backward

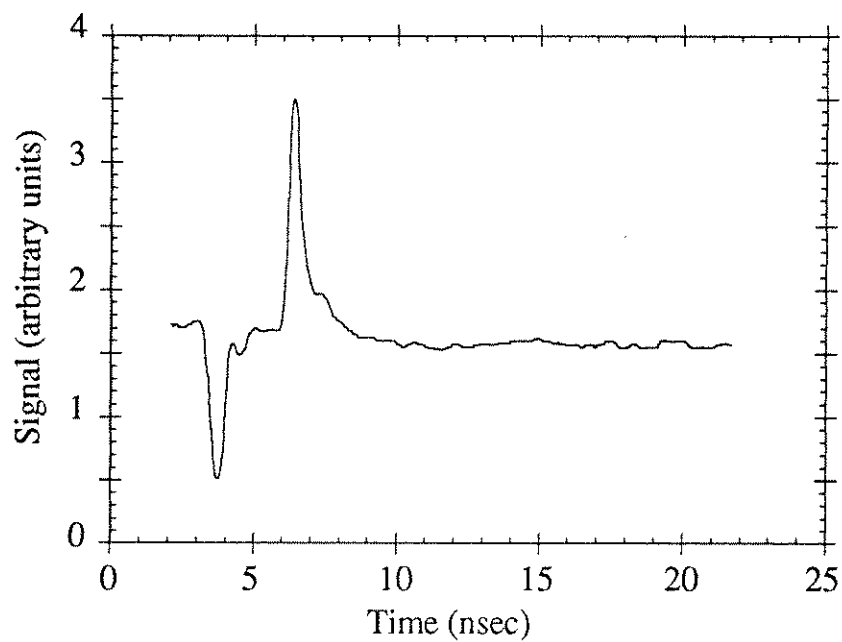


Figure 3.23: Backward upshifted signal recorded with a 36 GHz cutoff detector in the backward direction at 16 mT azulene pressure. The trailing edge of the pulse has decayed leaving a 1-nsec peak at the leading edge.

## Bibliography

- [1] J. D. Jackson, *Classical Electrodynamics*, Second Edition. New York: Wiley, p. 521, 1975.
- [2] V. I. Semenova, "Reflection of electromagnetic waves from an ionization front," *Sov. Radiophys. and Quantum Electron.*, vol. 10, pp. 599-604, 1967.
- [3] M. Lampe, E. Ott, and J. H. Walker, "Interaction of electromagnetic waves with a moving ionization front," *Phys. Fluids*, vol. 21, pp. 42-54, 1978.
- [4] W.B. Mori, "Generation of tunable radiation using an underdense ionization front," *Phys. Rev. A*, vol. 44, pp. 5118-5121, 1991.
- [5] E. Yablonavitch, "Self-phase modulation of light in a laser-breakdown plasma," *Phys. Rev. Lett.*, vol. 32, pp. 1101-1104, 1974.
- [6] P. B. Corkum, "High-power, subpicosecond 10- $\mu\text{m}$  pulse generation," *Opt. Lett.*, vol. 8, pp. 514-516, 1983.
- [7] W. M. Wood, C. W. Siders, and M. C. Downer, "Measurement of femtosecond ionization dynamics of atmospheric density gases by spectral blueshifting," *Phys. Rev. Lett.*, vol. 67, pp. 3523-3526, 1991.

- [8] S. C. Wilks *et al.*, "Photon accelerator," *Phys. Rev. Lett.*, vol. 62, pp. 2600-2603, 1989.
- [9] E. Esarey, G. Joyce, and P. Sprangle, "Frequency up-shifting of laser pulses by copropagating ionization fronts," *Phys. Rev. A*, vol. 44, pp. 3908-3911, 1991.
- [10] P. Sprangle, E. Esarey, and A. Ting, "Nonlinear interaction of intense laser pulses in plasmas," *Phys. Rev. A*, vol. 41, pp. 4463-4469, 1990.
- [11] H. C. Kapteyn and M. M. Murnane, "Relativistic pulse compression," *J. Opt. Soc. Am. B*, vol. 8, pp. 1657-1662, 1991.
- [12] V. B. Gil'denburg, A. V. Kim, and A. M. Sergeev, "Possibility of sharp increase in the frequency of the radiation of ionizing laser pulse in gas," *JETP Lett.*, vol. 51, pp. 104-107, 1990.
- [13] S. C. Wilks, J. M. Dawson, and W. B. Mori, "Frequency up-conversion of electromagnetic radiation with use of an overdense plasma," *Phys. Rev. Lett.*, vol. 61, pp. 337-340, 1988.
- [14] C. J. Joshi *et al.*, "Demonstration of the frequency upshifting of microwave radiation by rapid plasma creation," *IEEE Trans. Plasma Sci.*, vol. 18, pp. 814-818, 1990.
- [15] S. P. Kuo, "Frequency up-conversion of microwave pulse in a rapidly growing plasma," *Phys. Rev. Lett.*, vol. 65, pp. 1000-1003, 1990.
- [16] S. Ramo, J. R. Whinnery, and T. Van Duzer, *Fields and Waves in Communication Electronics*, Second Edition. New York: Wiley, p. 425, 1984.



- [17] D. Kalluri and R. K. Shrivastava, "Electromagnetic wave interaction with moving bounded plasmas," *J. Appl. Phys.*, vol. 44, pp. 4518-4521, 1973.